11. SITES 1008/1009[1]

Shipboard Scientific Party[2]

HOLE 1008A

Position: 23°36.64′N, 79°5.01′W

Start hole: 0100 hr, 4 April 1996

End hole: 1515 hr, 4 April 1996

Time on hole: 14 hr, 15 min

Seafloor (drill pipe measurement from rig floor, mbrf): 448.9

Total depth (drill pipe measurement from rig floor, mbrf): 583.4

Distance between rig floor and sea level (m): 11.8

Water depth (drill pipe measurement from sea level, m): 437.1

Penetration (mbsf): 134.5

Coring totals:
Type: APC; No: 10; Cored: 78.7 m; Recovered: 100.7%
Type: XCB; No: 6; Cored: 55.8 m; Recovered: 12.3%

Formation:
Unit I: 0–78.2 mbsf; Holocene to latest Pleistocene
Unlithified bioclastic and peloidal mudstone, wackestone, and packstone with intercalations of grainstones and floatstones
Unit II: 78.2–134.5 mbsf; Pleistocene
Unlithified lithoclastic and bioclastic floatstones, unlithified peloidal to bioclastic wackestones and lithified bioclastic packstones

HOLE 1009A

Position: 23°36.84′N, 79°3.00′W

Start hole: 1700 hr, 4 April 1996

End hole: 1600 hr, 5 April 1996

Time on hole: 23 hr

Seafloor (drill pipe measurement from rig floor, mbrf): 319.7

Total depth (drill pipe measurement from rig floor, mbrf): 545.8

Distance between rig floor and sea level (m): 11.8

Water depth (drill pipe measurement from sea level, m): 307.9

Penetration (mbsf): 226.1

Coring totals:
Type: APC; No: 16; Cored: 113.8 m; Recovered: 87.3%
Type: XCB; No: 12; Cored: 112.3 m; Recovered: 69.6%

Formation:
Unit I: 0–147.15; Holocene to latest Pleistocene
Unlithified bioclastic and peloidal mudstone, wackestone, and packstones
Unit II: 147.15–226.1 mbsf; Pleistocene
Partially lithified bioclastic mudstone to wackestone and partially lithified lithoclast floatstone

Principal results: The primary objective of Sites 1008 and 1009 was to obtain heat flow and interstitial water geochemistry measurements from a second area of the margin of the Great Bahama Bank to be used to compare with data from Sites 1003–1007. This approach was necessary to help support our findings regarding fluid flow and diagenetic reactions in the margin of the platform. A secondary objective was to retrieve a high-resolution section of Pleistocene–Holocene sediment for the study of recent climate change.

Sites 1008 and 1009 penetrated thick Pleistocene sections. At Site 1008, the age at the base of the hole (134.5 mbsf) is 1.44 Ma, with sedimentation rates varying between 4.5 and 16 cm/k.y. At Site 1009 a similar age was attained at a depth of 226.1 mbsf with sedimentation rates between 5 and 55 cm/k.y. Eight seismic sequences can be recognized in the drilled section that are separated from each other by seven seismic sequence boundaries (SSB). The strata at Sites 1008 and 1009 consist of lithified to partially lithified peloidal and bioclastic mudstones, wackestones, packstones, and grainstones with interbedded foraminifer nannofossil ooze. Most of the SSBs correlate with distinct layers in the cores that are dark in color, coarse-grained, and show signs of submarine cementation. Adara and WSTP temperature measurements revealed an irregular heat flux in the upper 40 mbsf and a much lower heat flux (20 mW vs. 40 mW) in the lower portion of the profile compared to Sites 1003–1007. Pore-water geochemistry profiles showed little variation in the upper 30 mbsf. Below this zone, sulfate reduction and other diagenetic reactions were prevalent. Two major lithologic units were distinguished at both Sites 1008 and 1009.

Unit I (0–78.2 mbsf, Site 1008; 0–147.15 mbsf, Site 1009) is Holocene to latest Pleistocene in age. Subunit IA (0–27.1 mbsf, Site 1008; 0–22.02 mbsf, Site 1009) consists of a coarsening-upward, pale yellow to white, unlithified peloidal wackestone grading into wackestone and mudstone, with minor to moderate bioturbation. The base of this subunit is marked in both sites by a bored and encrusted hardground. Subunit IB (27.1–78.2 mbsf, Site 1008; 22.02–98.71 mbsf, Site 1009) consists of multiple coarsening-upward sequences separated by harder layers. The sequences are composed of unlithified peloidal mudstones at the base and peloidal packstones at the top, which also correspond to cycles in physical properties. Characteristically they have relatively low velocities, densities, and gamma-ray values at their base that increase toward the top. The floatstones contain large gray lithoclasts composed of pteropod and planktonic foraminifer wackestone to packstone. The clasts are cemented and bored and are interpreted as being a remnant of a marine hardground. Subunit IC (98.71–147.15, Site 1009) was not recognized at Site 1008. It contains four coarsening-upward intervals and is separated from Subunit IB by a fragmented hard layer consisting of pteropod bioclastic packstone. Subunit IA at Site 1008 has a sedimentation rate of 4.5 cm/k.y. Subunit IB has a rate of 16 cm/k.y. At Site 1009, the sedimentation rates are 18 cm/k.y. throughout Subunit IA, up to 35 cm/k.y. in Subunit IB, and 7 cm/k.y. in Subunit IC.

Unit II (78.2–134.5, Site 1008; 147.15–226.1, Site 1009) consists of unlithified lithoclastic and bioclastic floatstone. At Site 1009, two hardgrounds are recognized in this sequence. At Site 1008, the sedimentation

[1]Eberli, G.P., Swart, P.K., Malone, M.J., et al., 1997. *Proc. ODP, Init. Repts.*, 166: College Station, TX (Ocean Drilling Program).
[2]Shipboard Scientific Party is given in the list preceding the Table of Contents.

Previous Chapter Table of Contents Next Chapter

rate in Unit II is 8 cm/k.y. At Site 1009 sedimentation rates are between 22 and 55 cm/k.y. throughout Unit II.

In both sites a number of alternations in sediment composition, color, and mineralogy can be recognized, probably corresponding to sea-level changes. Lowstands are characterized by higher concentration of low-magnesium calcite (LMC) and darker color compared to highstands that contain abundant aragonite and high-magnesium calcite (HMC). Dolomite becomes a minor component of the sediment below 60 mbsf in Site 1008 and 120 mbsf at Site 1009 and percent carbonate was generally higher than 95% throughout.

Sites 1008 and 1009 recovered extremely expanded sections of Holocene and Pleistocene sediments. The nannofossil biostratigraphy indicates the presence of Zones NN19 to NN21. The planktonic foraminifer record is restricted to N22. Substantial reworking was found in the lower part of the record.

The youngest seismic Sequence *s* appears at Site 1009 at 29 mbsf and at Site 1008 at 9.6 mbsf. The age of the SSB (0.15–0.12 Ma) probably corresponds to the last sea-level lowstand at the Pleistocene/Holocene boundary. SSB T corresponds to 48 mbsf at Site 1009 and 14.5 mbsf at Site 1008 and has an age of 0.20 to 0.25 Ma. These two boundaries, as well as SSB U, appear in both holes slightly deeper than high-velocity layers, allowing for the possibility that too high a velocity was assumed for these sediments in the time-depth conversions. Sequence *w* has its lower boundary at 126 and 53.2 mbsf at Sites 1009 and 1008, respectively. The associated age of SSB W, which might correlate to a high velocity layer 13 m higher in the core, is 0.7/0.62 Ma. The remainder of the holes show two prominent velocity deviations coinciding with SSBs X and Y.

Based on the pore-water geochemistry, two distinct geochemical zones have been identified within Sites 1008 and 1009. An upper zone, extending from the seafloor to a of depth 40 mbsf, is characterized by an absence of significant changes in the interstitial pore-water geochemistry. This flushed zone is similar to those observed at Sites 1006 and 1007, in that there was slight evidence of carbonate recrystallization reactions in the form of small increases in the Sr^{2+} concentration. Sites 1003, 1004, and 1005 showed no evidence of such an increase. The upper zone gradually merges into a region with elevated chlorinity, up to 730 mM at Site 1009 and 670 mM at Site 1008. This zone shows a small reduction in SO_4^{2-} and large increases (up to 1600 µM) in Sr^{2+}. Calcium and magnesium are reduced relative to their seawater values in this interval, suggesting precipitation of carbonate minerals. Methane and hydrogen sulfide reached concentrations of 100 and 10,000 ppm, respectively, within the zone with low sulfate.

Heat flow at both sites is significantly lower than at Sites 1003–1007. At Sites 1008 and 1009, the geothermal gradient is approximately 27°C/km and 17°C/km, respectively. This compares to approximately 35°C/km for the northern sites. The low heat flow could suggest a regional cooling as a result of the inflow of bottom seawater perhaps deeper in the sedimentary section.

BACKGROUND AND OBJECTIVES

Sites 1008 and 1009 are located approximately 100 km south of the Bahamas Transect sites (1003–1007) (Fig. 1). Site 1008 is situated in 437.1 m of water (23°36.640′N; 79°5.010′W) approximately 7.2 km from the platform edge as defined by the 10 fathom (18.83 m) contour line on seismic Line FS4 (Figs. 2, 3). Site 1009 (23°26.861′N; 79°03.027′W) is positioned in 307.9 m of water 2.7 km east of Site 1008, closer to the platform margin, near the junction of seismic Lines FS4 and FS2. Drilling at Site 1008 penetrated 134.5 m of Pleistocene-aged sediments, whereas Site 1009 drilled 226.1 m of Pleistocene deposits.

The principal objective of drilling at Sites 1008/1009 was to compare fluid flow in a different type of marginal setting (in terms of slope angle and depositional rate) compared to the northern sites. A secondary objective was to retrieve a high-resolution section of Holocene sediment for determining climate change. The original target depth for both sites was 250 mbsf.

The water column on the Great Bahama Bank (GBB) at this location is approximately two times deeper than at the position of the Western Geophysical seismic line (Western Line) and slopes more

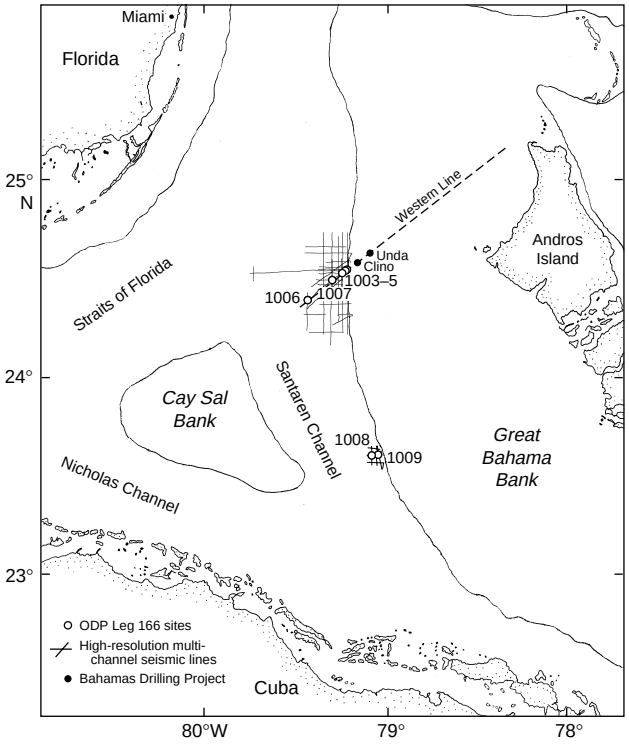

Figure 1. Location of Sites 1008 and 1009 relative to the northern Bahamas Transect sites.

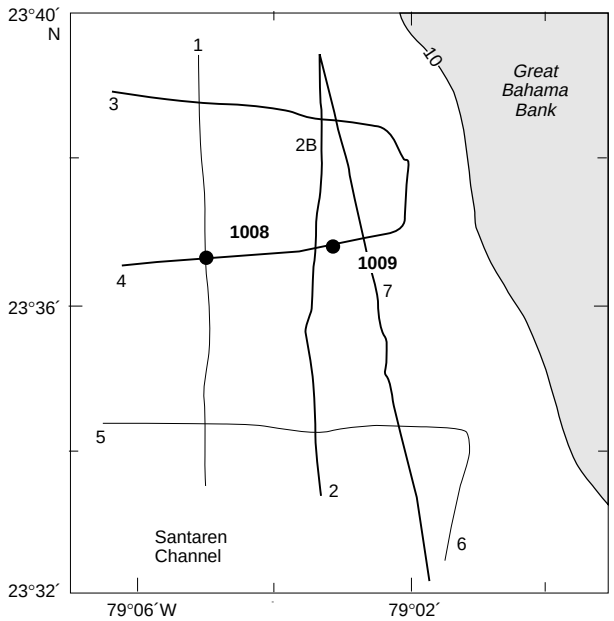

Figure 2. Location of Sites 1008 and 1009, on seismic Line 4 (numbered).

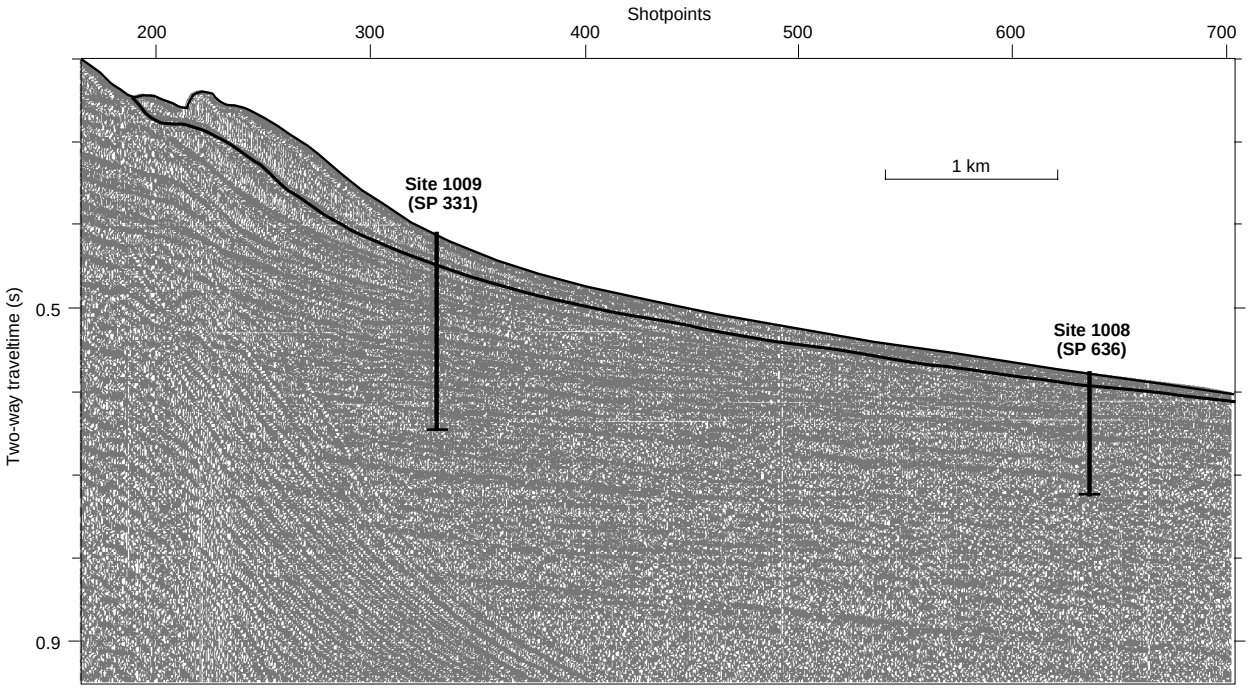

Figure 3. Single-channel seismic section along seismic Line FS4 displaying the prograding Quaternary sequences penetrated at Sites 1008–1009. The seismic line represents the image of the first trace of a MCS line. With this display, the high frequency (25–500 Hz) is preserved, which enables the reproduction of these sequences. The Holocene onlapping wedge is outlined.

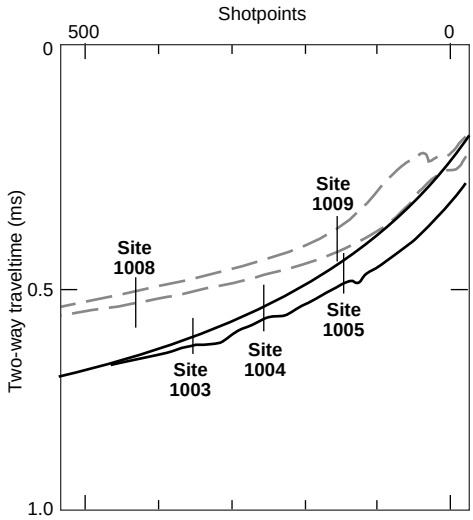

Figure 4. Comparison of slopes of the northern (solid lines) and southern (dashed lines) sites. The approximate position of the Holocene at each location is denoted by the lower line.

gradually to a depth of 100 m where a small terrace is found (Fig. 4). The main slope starts at this depth. In contrast, at the northern sites, the water depth increases much more rapidly, from 20 to 660 m. As a result of the different slope topography of this area, it was postulated that fluid recharge into the platform might be reduced or even absent in Sites 1008/1009. Previous seismic studies at this location have discovered a thick sequence of carbonate muds, believed to be of Holocene age, overlying the Pleistocene (Wilber et al., 1990). This thick succession was an ideal target to retrieve a high-resolution record of the Holocene.

As at the previous sites, the presence of fluid flow was documented using a combination of temperature and geochemical measurements. Temperature was measured using the Adara heat flow tool from Core 3H until refusal, and after that the WSTP tool was used every third core. Water samples were taken on every other section in the upper two cores and on every core thereafter, recovery permitting.

OPERATIONS

Transit

The 55-nmi sea voyage from Site 1007 to Site 1008 was made in 4.75 hr. A stand of drill collars was inspected during the transit, and an APC BHA was assembled. A Datasonics 354M beacon was dropped at 0105 hr on 4 April.

Hole 1008A

Hole 1008A was spudded at 0339 hr on 4 April. The water depth was 437.1 mbsl based on recovery of the mudline core. APC Cores 1008A-1H through 10H were taken from 0 to 78.7 mbsf with 100.7% recovery (Table 1). Adara heat flow measurements were performed on Cores 3H through 8H. The same cores also were oriented. A hard layer was drilled from 34.1 to 35.1 mbsf. Core 9H required 80,000-lb overpull after washing for 3 min. Core 10H refused to advance into a carbonate gravel; therefore, XCB coring was initiated. XCB Cores 11X through 16X were cut from 78.7 to 134.5 mbsf with 12.3% average recovery. The WSTP was deployed after Core 14X. XCB recovery was very poor in soft sediments with sporadic hard layers.

Table 1. Sites 1008/1009 coring summaries.

Core	Date (Apr 1996)	Time (UTC)	Depth (mbsf)	Length cored (m)	Length recovered (m)	Recovery (%)
166-1008A-						
1H	4	0850	0.0–6.6	6.6	6.6	100.0
2H	4	0910	6.6–16.1	9.5	9.5	100.0
3H	4	1000	16.1–25.6	9.5	10.1	105.9
4H	4	1040	25.6–35.1	9.5	10.1	105.8
5H	4	1125	35.1–40.2	5.1	4.1	80.4
6H	4	1215	40.2–49.7	9.5	9.7	102.0
7H	4	1305	49.7–59.2	9.5	9.6	101.0
8H	4	1405	59.2–68.7	9.5	9.9	104.0
9H	4	1445	68.7–78.2	9.5	9.2	97.1
10H	4	1510	78.2–78.7	0.5	0.5	98.0
11X	4	1610	78.7–88.1	9.4	3.0	31.6
12X	4	1655	88.1–97.4	9.3	0.0	0.0
13X	4	1725	97.4–106.8	9.4	0.0	0.0
14X	4	1840	106.8–116.1	9.3	0.1	1.1
15X	4	1905	116.1–125.3	9.2	6.7	73.2
16X	4	1925	125.3–134.5	9.2	0.0	0.0
Coring totals				134.5	89.1	66.2
166-1009A-						
1H	4	2330	0.0–4.8	4.8	4.8	99.4
2H	5	0000	4.8–14.3	9.5	9.3	97.6
3H	5	0045	14.3–23.8	9.5	7.9	83.6
4H	5	0130	23.8–33.3	9.5	4.7	49.0
5H	5	0210	33.3–38.3	5.0	4.8	96.4
6H	5	0255	38.3–42.3	4.0	1.1	26.2
7H	5	0405	42.3–51.8	9.5	9.4	99.0
8H	5	0430	51.8–61.3	9.5	9.8	103.0
9H	5	0450	61.3–70.8	9.5	9.7	102.0
10H	5	0520	70.8–73.8	3.0	1.3	42.0
11H	5	0630	73.8–83.3	9.5	8.5	89.0
12H	5	0705	83.3–86.3	3.0	1.0	34.0
13H	5	0725	86.3–95.8	9.5	9.6	101.0
14H	5	0855	95.8–105.3	9.5	9.1	95.6
15H	5	0915	105.3–111.8	6.5	6.5	100.0
16H	5	0945	111.8–113.8	2.0	1.9	96.5
17X	5	1025	113.8–123.5	9.7	7.2	74.3
18X	5	1140	123.5–132.9	9.4	2.2	23.8
19X	5	1200	132.9–142.5	9.6	7.2	75.1
20X	5	1230	142.5–152.0	9.5	5.2	54.7
21X	5	1345	152.0–161.5	9.5	0.0	0.2
22X	5	1410	161.5–170.8	9.3	5.6	60.5
23X	5	1430	170.8–180.1	9.3	8.1	86.0
24X	5	1540	180.1–189.4	9.3	9.6	103.0
25X	5	1600	189.4–198.5	9.1	9.6	105.0
26X	5	1620	198.5–207.6	9.1	7.3	80.5
27X	5	1645	207.6–216.7	9.1	9.9	108.0
28X	5	1710	216.7–226.1	9.4	7.9	83.5
Coring totals				226.1	179.2	79.3

Note: An expanded version of this coring summary table that includes lengths and depths of sections, location of whole-round samples, and comments on sampling disturbance is included on CD-ROM in the back pocket of this volume.

Coring was terminated when the available operating time for this site was depleted. The bit cleared the seafloor at 1520 hr on 4 April.

Transit

The 1.8-nmi transit to Site 1009 was made in dynamic positioning mode with the BHA suspended at 250 mbrf. A Datasonics 354M beacon was dropped at 1658 hr on 4 April. The drill site was moved about 73 m east of the originally proposed site coordinates to obtain a thicker Holocene section.

Hole 1009A

Hole 1009A was initiated at 1825 hr on 4 April. The water depth was 307.9 mbsl based on recovery of the mudline core. APC Cores 1009A-1H through 16H were taken from 0 to 113.8 mbsf with 99.3% average recovery. Adara heat flow measurements were performed on Cores 3H through 7H. The same cores were also oriented. A hard layer was drilled from 22.0 to 23.5 mbsf. Core 7H was a full stroke that would not pull free with 50,000-lb overpull and was drilled over 6 m. The APC was advanced as far as possible; however, six cores had imploded tops or shattered liners and seven of 16 cores were partial strokes because of the occurrence of sporadic hard layers. Consequently, we switched to the XCB coring system after Core 16H. XCB Cores 17X through 28X were cut from 113.8 to 226.1 mbsf with 69.6% recovery. Four of 12 XCB cores were jammed in the liner or core catcher. The WSTP was deployed after Cores 11X, 14X, 18X, 21X, and 24X. Coring was terminated when the available time was depleted. The BHA was secured for sea voyage at 1600 hr on 5 April.

Sea Voyage to Panama

The sea voyage from Site 1009 to Panama covered 1100 nmi in about 95.6 hr. Leg 166 ended with the first line ashore in Panama at 1600 hr, 10 April.

LITHOSTRATIGRAPHY

Site 1008

Lithologic Units

A succession of 134.5 m of Pleistocene sediments was recovered at Site 1008 (Fig. 5), for an average recovery of 66.2%. The deposits consist of unlithified mudstone, wackestone, packstone, and grainstone with interbedded foraminifer nannofossil ooze and floatstone, and one thin clay-rich layer. Methods used to describe the sedimentary succession include visual core descriptions, determination of silt- to sand-sized allochems in wash samples, and smear-slide analyses. Smear-slide analyses indicate that the occurrence of aragonite needles, peloids, and nannofossils varies throughout Site 1008 (Fig. 6). Throughout the entire hole, silt- to fine sand-sized peloids are the dominant allochem. Benthic foraminifers, *Halimeda*, and bioclasts also occur. All deposits are unlithified except for some partially lithified sediments in Unit I and some lithified sediments at the base of Unit II. The succession at Site 1008 was divided into two subunits on the basis of compositional and textural changes.

Unit I

Interval: 166-1008A-1H through 10H-1
Age: Pleistocene
Depth: 0–78.2 mbsf

Unit I consists of unlithified mudstone, wackestone, packstone to floatstone, and nannofossil ooze. A lithologic change from unlithified mudstone to wackestone with abundant peloids, bioclasts, and millimeter-scale laminations to unlithified lithoclastic floatstone and bioclastic floatstone defines the contact between Units I and II (top of Section 166-1008A-10H-1). Unit I is divided into two subunits on the basis of sediment composition, the distribution of hardgrounds, and debris flows. Subunits IA and IB, which are separated by a thick bed of nannofossil ooze in Core 166-1008A-4H, each contain three coarsening-upward successions. The contacts between the individual coarsening-upward cycles in Subunit IA are placed on top of debris-flow deposits and a hardground, respectively (Sections 166-1008A-1H-5 and 2H-4).

Subunit IA

Interval: 166-1008A-1H through 5H-3, 55 cm
Age: Pleistocene
Depth: 0–27.1 mbsf

Subunit IA consists of an upper interval of light gray unlithified peloidal foraminifer wackestone that grades downhole into white unlithified peloidal wackestone to mudstone. The occurrence of a layer

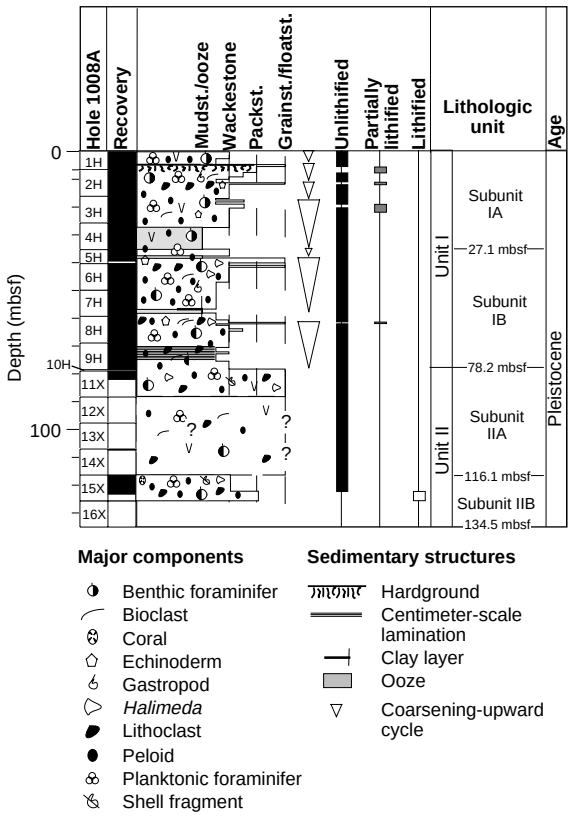

Figure 5. Synthesis of the dominant textures and components of the sedimentary succession at Site 1008.

consisting of lithified clasts that are bored and encrusted marks the base of the first coarsening-upward sequence (Sections 166-1008A-1H-5 through 2H-1). The top of the second coarsening-upward sequence consists of a light olive gray unlithified floatstone. The lithoclastic floatstone overlies light gray to pale yellow unlithified peloidal packstone to wackestone that grades downhole into unlithified peloidal wackestone to mudstone. Light olive gray unlithified floatstone with burrowed lithoclasts (Section 166-1008A-2H-3, 68 cm) defines the top of a third sequence and overlies white, light gray, and pale yellow, unlithified wackestone and wackestone to mudstone. The fourth and lowermost sequence in Subunit IA consists of white, light gray, pale yellow, and light olive brown, partially lithified and unlithified biowackestone to biowackestone grading down to unlithified foraminifer and peloidal wackestone and nannofossil ooze. Silt- to sand-sized allochems include peloids, planktonic and benthic foraminifers, and bioclasts.

The peloid-dominated sediment in the upper part of Subunit IA is characterized by variable bioturbation, which is visible as distinct burrows filled with fine-grained, grayish to darker yellowish sediment. Allochems are silt-sized peloids, benthic and planktonic foraminifers, bioclasts, pteropods, echinoderm spines, rare ostracodes, tunicates, some phosphatic grains and shell fragments, and pebble-sized packstone lithoclasts with pteropods, planktonic foraminifers, gastropods, and bioclasts. Pale yellow to light gray nannofossil ooze, which composes the lowermost part of Subunit IA, is moderately bioturbated. Bioturbation appears as color mottles and contains burrows filled with black grains. Major allochems are sand-sized planktonic and benthic foraminifers, peloids, sponge spicules, bioclasts, echinoderm debris, ostracodes, and rare shark teeth.

Subunit IB

Interval: 166-1008A-5H-3, 55 cm, through 9H-CC, 80 cm
Age: Pleistocene
Depth: 27.1–78.2 mbsf

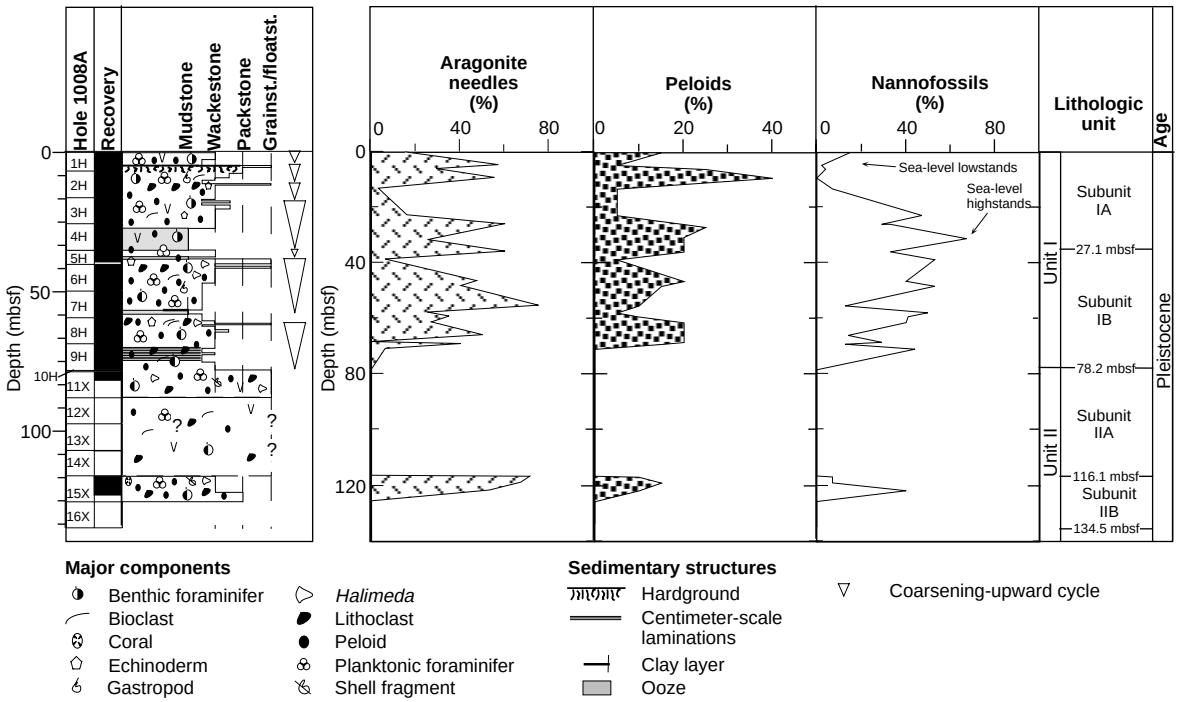

Figure 6. Comparison of smear-slide estimates of percent aragonite needles, peloids, and nannofossils vs. depth at Site 1008.

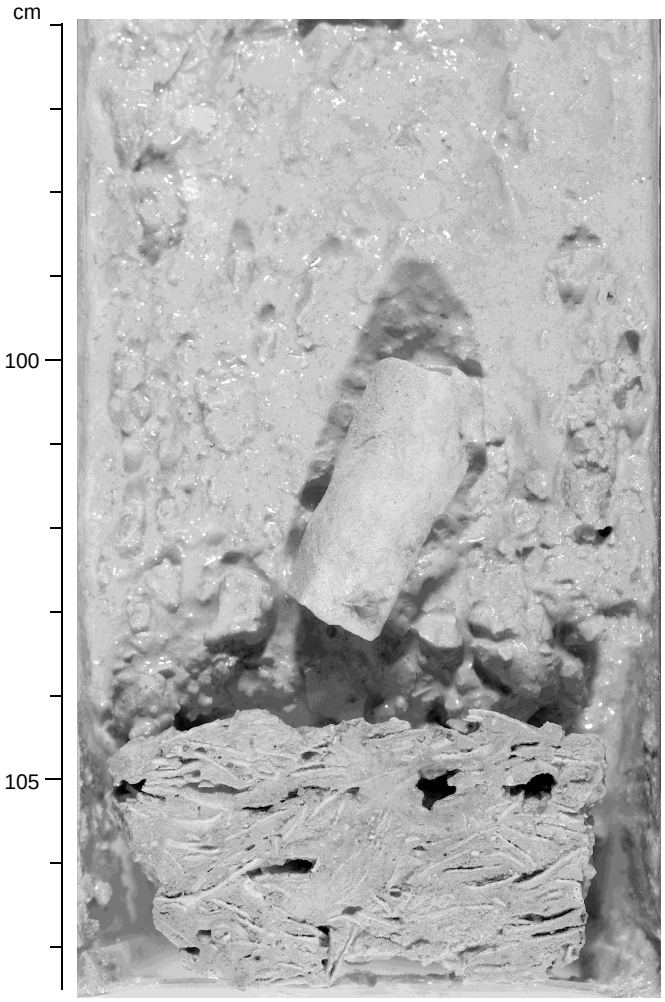

Figure 7. Detail of a *Halimeda*-rich lithoclastic floatstone with a *Halimeda* wackestone and a lithified burrow, which defines the upper contact of Subunit IB in interval 166-1008A-5H-3, 96–107.5 cm.

Subunit IB consists of three coarsening-upward sequences. The uppermost sequence contains pale yellow unlithified peloidal wackestone changing downhole to foraminifer nannofossil ooze and packstone cobbles. The first pale yellow unlithified *Halimeda* floatstone (Fig. 7) with pieces of bored Halimeda grainstone defines the upper contact of the middle sequence in Subunit IB (Section 166-1008A-5H-3, 5 cm). The upper floatstone is separated from a second light gray lithoclastic floatstone by a 40-cm-thick, white layer of unlithified foraminifer wackestone. The lithoclastic floatstone, which is rich in Halimeda and foraminifers, grades downhole into unlithified peloidal wackestone and unlithified peloidal wackestone to mudstone with nannofossils. A black, clay-rich layer occurs at the top of a light gray nannofossil ooze with foraminifers, which defines the base of the second sequence (Section 166-1008A-7H-6, 73 cm). Pale yellow and white unlithified peloidal mudstone to wackestone, which grades down into wackestone and unlithified to partially lithified floatstone with echinoderms and shell fragments, defines the top of the last sequence in Subunit IB. The lowermost coarsening-upward sequence consists in the upper portion of light greenish gray to pale yellow peloidal wackestone, which changes downhole to unlithified peloidal wackestone to mudstone and wackestone to packstone. It is underlain by peloidal wackestone above unlithified mudstone to wackestone, which grades downhole into peloidal wackestone.

The pale yellow to light gray peloidal mudstone to wackestone and peloidal wackestone deposits that compose the bulk of Subunit IB show moderate bioturbation, which appears as grayish to black color mottling. Well-defined burrows occur only in Core 166-1008A-8H. Pale olive to pale yellow mudstone to wackestone at the bottom of the lowermost sequence displays very fine laminations of light-colored, aragonite-rich vs. darker colored, micrite-rich layers (Sections 166-1008A-9H-5 through 9H-6).

The unlithified peloidal wackestone and mudstone to wackestone in Subunit IB contain silt- to sand-sized benthic and planktonic foraminifers, lithoclasts, bioclasts, echinoderm debris, gastropods, minor fish debris, tunicates, sponge spicules, and blackened grains. The encrusted grainstone to packstone lithoclasts contain peloids, planktonic foraminifers, coral debris, and bryozoa. Yellowish nannofossil ooze, which is slightly bioturbated, contains planktonic and benthic foraminifers, echinoderm spines, and gastropods.

Unit II

Interval: 166-1008A-10H through 16X
Age: Pleistocene
Depth: 78.2–134.5 mbsf

Unit II consists of unlithified lithoclastic and bioclastic floatstone, unlithified peloidal to bioclastic wackestone, and lithified bioclastic packstone. In this unit, dominant silt- to sand-sized allochems are primarily bioclasts and peloids. Smear-slide analyses indicate that the aragonite content of the peloidal to bioclastic wackestone and packstone reaches 40%–50% in Core 166-1008A-15X (Fig. 6). Lithoclastic floatstone occurs in Cores 166-1008A-10H through 11X, but there was no recovery in Cores 166-1008A-12X, 13X, and 16X. The unrecovered interval might also consist of lithoclastic floatstone, as this entire interval consists of a similar seismic transparent facies (see "Seismic Stratigraphy" section, this chapter). The disappearance of floatstone and the appearance of bioclastic wackestone at the top of Core 166-1008A-15X defines the contact between Subunits IIA and IIB.

Subunit IIA

Interval: 166-1008A-10H through 14X
Age: Pleistocene
Depth: 78.2–116.1 mbsf

Subunit IIA consists of white to light green unlithified lithoclastic and bioclastic floatstone. Sand-sized allochems include planktonic and benthic foraminifers, shell fragments, pteropods, and phosphatic grains. A few centimeter-thick beds of pale yellow, partially lithified to unlithified mudstone to wackestone are interbedded in Section 166-1008A-11X-2, 15 cm. The unlithified lithoclastic floatstone in Section 166-1008A-11X-1 shows reverse grading and an upward increase in grain size and abundance of black grains, benthic foraminifers (miliolids), and lithoclasts.

Subunit IIB

Interval: 166-1008A-15X-1 through 16X
Age: Pleistocene
Depth: 116.1–134.5 mbsf

Subunit IIB consists of pale yellow, light green, light gray unlithified peloidal to bioclastic wackestone, which changes downhole to brownish bioclastic packstone. Silt- to sand-sized allochems are lithoclasts, planktonic and benthic foraminifers, *Halimeda*, shell fragments, bioclasts, coral fragments, and sponge spicules. Slight bioturbation appears as (1) greenish fine-grained structureless burrows, (2) indistinct, greenish burrows containing a higher abundance of coarse sand-sized pteropods and foraminifers than in the surrounding sediment, and (3) indistinct accumulations of phosphatic grains.

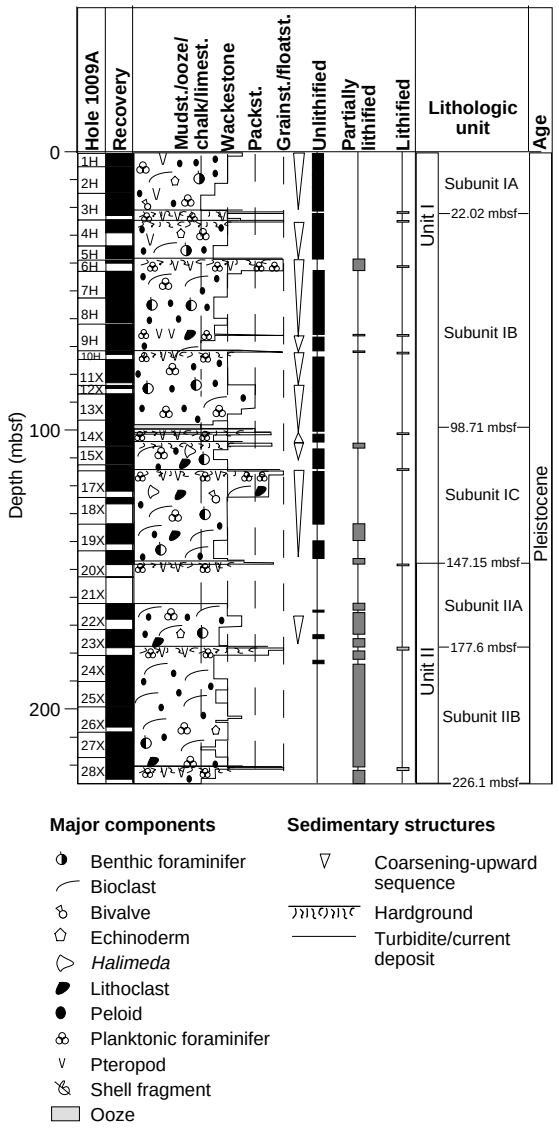

Figure 8. Synthesis of the dominant textures and components of the sedimentary succession at Site 1009.

Site 1009

Introduction

A 226.1-m succession of Pleistocene carbonate sediments was recovered at Site 1009 (Fig. 8). The sediments consist of unlithified to partially lithified peloidal and bioclastic mudstone, wackestone and packstone with grainstone, floatstone intercalations and a nannofossil ooze layer. Methods used to describe the sedimentary succession include visual core descriptions, sieve samples, and smear-slide analyses. Silt- to medium sand-sized peloids and bioclasts are abundant throughout the entire hole. Pteropods and planktonic foraminifers are more common in the floatstones. The occurrence of aragonite needles, peloids, and nannofossils shows distinct fluctuations at Site 1009 (Fig. 9). Carbonate content varies from 91% and 99% (see "Organic Geochemistry" section, this chapter). The sedimentary section recovered at Site 1009 is divided into two main subunits based on a downcore increase in degree of lithification, a decrease in the relative abundance of peloids, and the periodicity and definition of coarsening-upward cycles. The two units correspond to Unit I of Sites 1003, 1004, 1005, 1006, and 1007 defined previously based on the presence of peloids.

Description of Lithologic Units

Unit I

Interval: 166-1009A-1H through 20X
Age: Pleistocene
Depth: 0–147.15 mbsf

Unit I is characterized by multiple coarsening-upward sequences, each of which is capped by unlithified lithoclastic floatstones. These layers contain coarse sand- to gravel-sized blackened grains and gray, gravel- to cobble-sized lithoclasts that contain pteropods and foraminifers. All larger lithoclasts consist of pteropod- and foraminifer-rich lithoclasts, which are bored and encrusted at the top. Therefore, these layers may represent submarine hardgrounds that were fragmented during drilling (see Grammer and Ginsburg, 1992; figs. 6–10). The coarse intervals with blackened grains and gray lithoclasts are described as grainstones to floatstones. The coarsening-upward sequences grade upward from unlithified mudstone to wackestone, and successively to packstone. These sequences contain abundant peloids and bioclasts. In addition to the mixed pelagic and neritic lithologies, a nannofossil ooze was observed in Unit I (Section 166-1009A-14H-2).

The base of Unit I is marked by a lithologic change from an unlithified peloidal mudstone to wackestone to a partially lithified bioclastic mudstone to wackestone, a sharp color change combined with a decrease in peloid abundance, and an increase in bioclasts (Section 166-1009A-20X-4, 0.15 cm).

Unit I is divided into Subunits IA, IB, and IC on the basis of sediment composition and the distribution of hardgrounds. The subunits contain, respectively, one, five, and four coarsening-upward sequences capped by unlithified lithoclastic floatstones with clasts of several centimeters in diameter. The contact between Subunits IA and IB (Section 166-1009A-3H-6, 22 cm) is marked by the first unlithified lithoclastic floatstone encountered downhole. The contact between Subunits IB and IC is defined at the base of the only nannofossil ooze layer observed at Site 1009 (Section 166-1009A-14H-2, 141 cm).

Subunit IA

Interval: 166-1009A-1H through 3H-6, 22 cm
Age: Pleistocene
Depth: 0–22.02 mbsf

Subunit IA consists of a 22-m-thick, coarsening-upward sequence of white to pale yellow unlithified mudstone, wackestone, and peloidal packstone. The sediments display minor to moderate bioturbation, which is visible as color mottles and burrows that lack distinct margins. The first section of Subunit IA (166-1009A-1H-1) contains a biowackestone with a high concentration and diversity of grains. Grain diversity and abundance decreases below Section 166-1009A-1H-1. The silt- to fine sand-sized allochems are well sorted and consist primarily of peloids. Other allochems include benthic foraminifers, bioclasts, pteropods, planktonic foraminifers, echinoderm spines, gastropods, bivalve fragments, ostracodes, sponge spicules and intraclasts. Some brown planktonic foraminifers and bioclasts are observed at the top of the unit. The clay- to silt-sized fraction, which composes the sediment matrix, consists of aragonite needles and micrite. Calcareous nannofossils are rare or absent within most of the subunit.

Subunit IB

Interval: 166-1009A-3H-6, 22 cm, through 14H-2, 141 cm
Age: Pleistocene
Depth: 22.02–98.71 mbsf

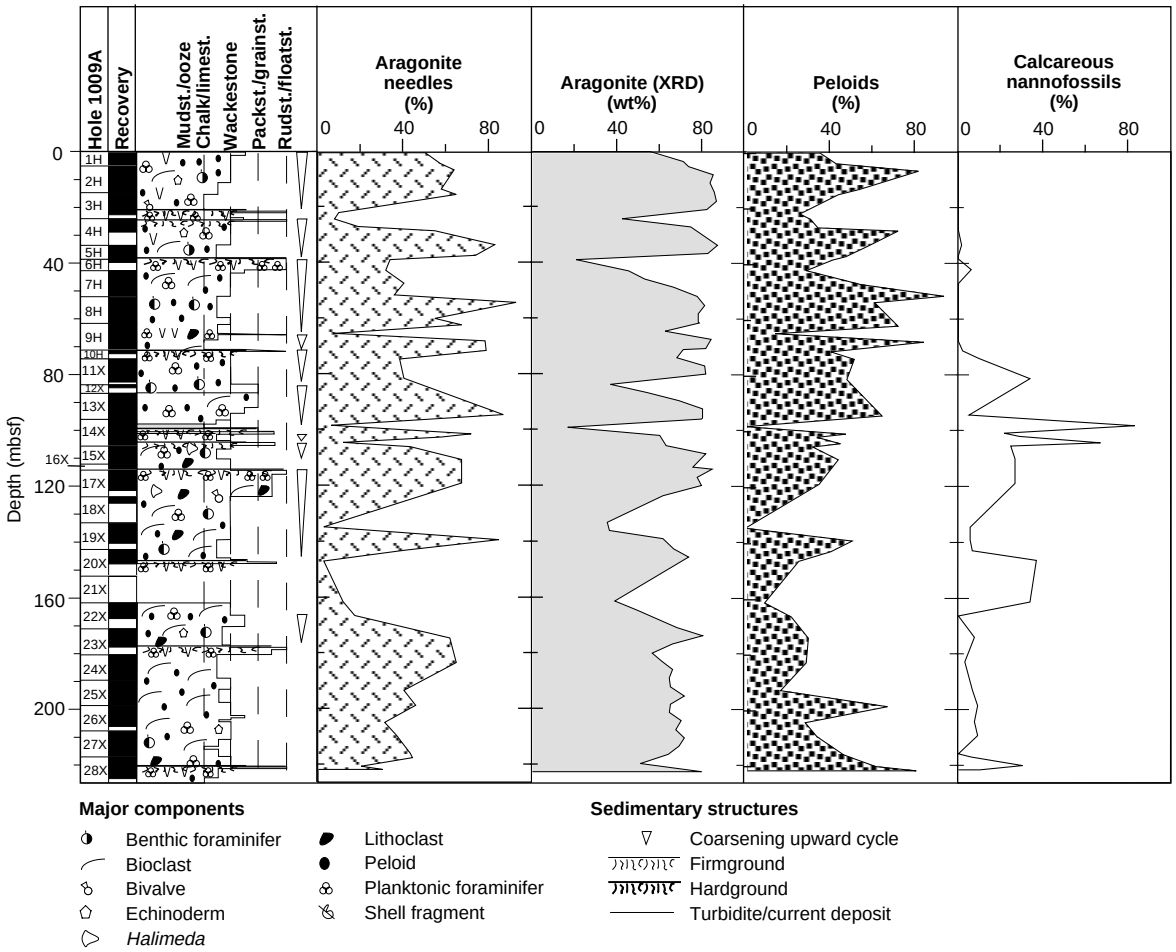

Figure 9. Comparison between aragonite needles, peloids, and calcareous nannofossils from smear-slide analyses, and weight percent aragonite from XRD for Site 1009.

Subunit IB consists of five coarsening-upward sequences, each of which is separated by layers of unlithified lithoclastic floatstones. The sequences are composed of unlithified peloidal mudstone at the base, unlithified peloidal wackestone in the middle, and unlithified peloidal wackestone to packstone at the top. Thicknesses of the sequences vary from about 3 to 20 m. The color of each sequence changes downcore from light olive brown, to pale yellow, to white. The color change coincides with an increase in grain diversity and a decrease in peloid abundance. In addition to peloids, silt- to fine sand-sized allochems are benthic and planktonic foraminifers, bioclasts, pteropods, ostracodes, echinoderm spines, and shell fragments. The clay- to silt-sized fraction consists of aragonite needles, micrite, and rare calcareous nannofossils.

The upper limit of Subunit IB (Section 166-1009A-3H-6, 22 cm) is marked by the top of an interval consisting of a light gray lithoclastic packstone to lithoclastic floatstone. The fine to coarse sand-sized fraction consists of planktonic and benthic foraminifers, pteropods, bioclasts, intraclasts, and lithoclasts. Fifty percent of the components are gray in color. The floatstone contains large (3–6 cm) gray lithoclasts that are made up of pteropod and planktonic foraminifer wackestone to packstone. The clasts are well-cemented and bored. Some are encrusted by serpulid worm tubes and bryozoans and contain geopetal infill (Fig. 10), and may represent a marine hardground. Three similar layers occur in Subunit IB (Sections 166-1009A-6H-1, 9H-3, and 10H-1, 83 cm); however, not all of them are as clearly expressed. Another possible hardground was found in interval 166-1009A-4H-1, 62–106 cm, that consists of a white peloidal packstone that is bored and encrusted by worm tubes at the top. This hard layer is associated with bivalves (*Glycimeris*, 1 cm size). A pale yellow to light gray nannofossil ooze (Section 166-1009A-14H-2) makes up the lowermost part of Subunit IB. Bioturbation is moderate to strong throughout the subunit and is visible as burrows filled with concentrations of black grains.

Subunit IC

Interval: 166-1009A-14H-2, 141 cm, through 20X-4, 15 cm
Age: Pleistocene
Depth: 98.71–147.15 mbsf

The top of Subunit IC (Section 166-1009A-14H-3, 60 cm) is an interval containing lithoclasts of pteropod planktonic foraminifer packstone encrusted by serpulid worm tubes and bryozoans. This interval may represent a submarine hardground. The benthic foraminifer *Lepidocyclina* is also present in this interval. Directly below this layer, a fining-upward interval (Section 166-1009A-14H-4, 0–57 cm) consisting of pale yellow to white unlithified bioclastic grainstone to wackestone (turbidite) occurs. This fining-upward interval contains fine- to coarse sand-sized peloids, planktonic foraminifers, shell fragments, encrusting foraminifers, echinoderm spines, and *Halimeda.*

The remainder of Subunit IC comprises three coarsening-upward sequences ranging in thickness from 3 to 30 m. The thickest of these

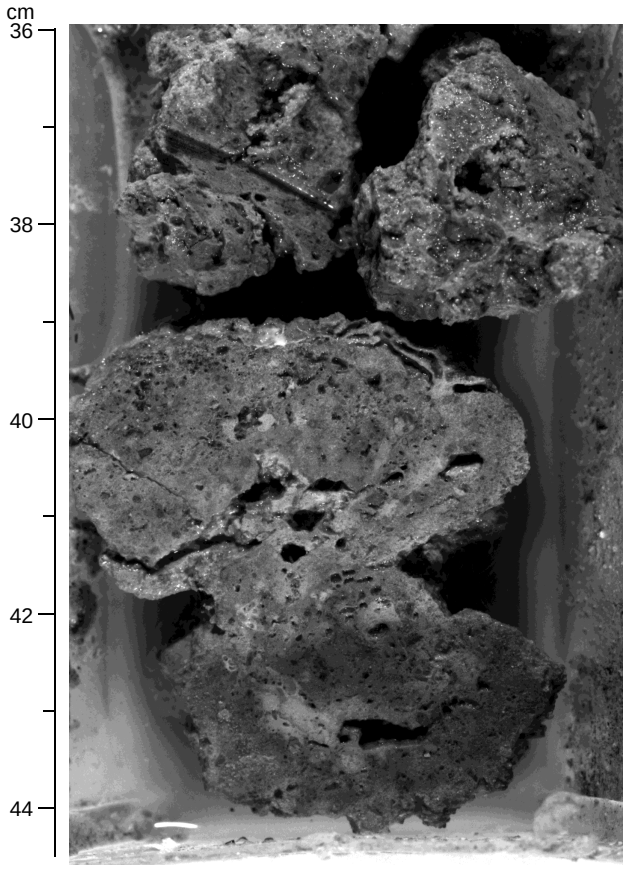

Figure 10. Close-up photograph of submarine hardground with encrusting bryozoans and serpulid worm tubes at the top and geopetal structures (interval 166-1009A-3H-6, 36–44.5 cm).

sequences (Sections 166-1009A-17X-1, 30 cm, to 20X-4, 15 cm) occurs below an interval containing lithoclasts of gray, pteropod planktonic foraminifer packstone to floatstone (Sections 166-1009A-17X-1, 0–30 cm). The thick, coarsening-upward sequence consists of a light gray unlithified bioclastic floatstone to packstone at the top, pale yellow unlithified bioclastic wackestone in the middle, and white unlithified bioclastic wackestone to mudstone at the base. The floatstone to packstone interval (Sections 166-1009A-17X-1, 30 cm, to 17X-CC, 26 cm) contains sand- to gravel-sized lithoclasts, *Halimeda* debris, gastropods, shell debris, and bivalves. The fine to coarse sand-sized fraction is made up of pteropods, benthic and planktonic foraminifers, peloids, and bioclasts. The clay- to silt-sized fraction consists of aragonite needles, micrite, and calcareous nannofossils. The base of Unit I is placed at the top of a lithoclast layer in Section 166-1009A-20X-4, 15 cm.

Unit II

Interval: 166-1009A-20X-4, 15 cm, through 28X
Age: Pleistocene
Depth: 147.15–226.10 mbsf

Unit II consists of partially lithified bioclastic mudstone to wackestone and partially lithified lithoclastic floatstone. The dominant silt- to sand-sized allochems are bioclasts, peloids, benthic foraminifers, and planktonic foraminifers. The clay- to silt-size fraction, which composes the matrix, consists of micrite and aragonite needles with minor amounts of calcareous nannofossils. Unit II is divided into Subunits IIA and IIB on the basis of sediment composition and the distribution of hardgrounds. The top of Unit II corresponds to a lithoclast layer in Section 166-1009A-20X-4, 15 cm, to 20X-CC, 43 cm. A second hard layer marks the boundary between Subunits IIA and IIB (interval 166-1009A-23X-5, 80–121 cm), and a third hard layer is included in Subunit IIB (interval 166-1009A-28X-3, 120–135 cm).

Subunit IIA

Interval: 166-1009A-20X-4, 43 cm, through 23X-5, 80 cm
Age: Pleistocene
Depth: 147.68–177.60 mbsf

Subunit IIA comprises a coarsening-upward sequence of pale olive, partially lithified bioclastic wackestone and unlithified peloidal packstone that grades downhole into a pale yellow, partially lithified bioclastic mudstone. Dominant sand-sized allochems include bioclasts and peloids. Planktonic foraminifers, intraclasts, and benthic foraminifers are also present. The clay- to silt-sized matrix constituents include micrite and minor amounts of aragonite needles and calcareous nannofossils. Moderate to strong bioturbation is pervasive throughout Subunit IIA.

The upper limit of Subunit IIA is placed at the top of a lithoclastic floatstone layer (Section 166-1009A-20X-4, 15 cm). Lithoclasts are composed of light gray, pteropod, planktonic foraminifer wackestone to packstone, similar to the hardgrounds defined in Unit I. This hard layer overlies a core with no recovery (Core 166-1009A-21X). A thin fining-upward interval occurs at the base of Subunit IIA (Section 166-1009A-23X-5, 80–100 cm). This interval shows a downcore increase in the number of gray planktonic foraminifers and pteropods, and represents a gradual transition to a lithoclastic floatstone that defines the upper limit of Subunit IIB.

Subunit IIB

Interval: 166-1009A-23X-5, 80 cm, through 28X
Age: Pleistocene
Depth: 177.60–226.10 mbsf

Subunit IIB consists of a monotonous alternation of pale yellow to white partially lithified bioclastic wackestone, bioclastic wackestone to mudstone, and bioclastic mudstone. The only lithologic change is in the grain abundance. In addition to bioclasts, dominant allochems include fine sand-sized peloids, benthic and planktonic foraminifers, echinoderm spines, intraclasts, and ostracodes. The clay- to silt-sized fraction, which comprises the matrix, consists of subequal amounts of micrite and aragonite needles, and minor amounts of calcareous nannofossils. Pervasive moderate to strong bioturbation is visible as faint color mottles, and as round structureless burrows filled with greenish sediments. Some burrows are partially lithified. A thin lithoclastic floatstone occurs in Section 166-1009A-28X-3, 120–135 cm.

Discussion

The sedimentary successions that make up lithologic Unit I at Sites 1008 and 1009 can be characterized as a series of coarsening-upward cycles, each of which is capped by a layer of unlithified lithoclastic floatstone. In general, these coarsening-upward trends result from an upward increase in the abundance of allochems and not from a significant increase in grain size. At Site 1008, the more distal of these two sites, the basal parts of cycles are typically composed of nannofossil ooze. These basal oozes are overlain by unlithified mudstones to wackestones that grade upward to unlithified peloidal or bioclastic wackestones to packstones. Lithoclastic floatstones with large bored and encrusted clasts form the tops of these coarsening-upward cycles. At Site 1009, cycles are virtually identical, except that they typically lack the basal nannofossil ooze observed at Site 1008.

This difference is probably due to the more proximal location of Site 1009.

Unit I depositional cycles found at Site 1008 can be correlated to those present at Site 1009 (Fig. 11). Correlation is based on percent color reflectance and the occurrence of unlithified lithoclastic floatstone layers that cap each coarsening-upward sequence. In addition, seismic sequence Boundaries S through V (see "Seismic Stratigraphy" section, this chapter) run parallel to the lithologic and color reflectance correlation lines. This correlation clearly shows the wedge-shaped geometry of the upper Quaternary depositional package, and indicates that the sedimentary succession at Site 1009 is expanded relative to that at Site 1008.

The intervals containing unlithified lithoclastic floatstone are generally disturbed during drilling. This makes interpretation of the relationship between the Unit I coarsening-upward cycles and sea level difficult. Many lithoclasts in the floatstones show all of the characteristic features of submarine hardgrounds, including multiple generations of cementation, boring, and sediment infill (e.g., Grammer and Ginsburg, 1992), whereas others resemble carbonate nodules that "float" in a muddy matrix and are similar to nodular oozes described north of the Great Bahama Bank (Mullins, 1983). Thus, recovered intervals of unlithified lithoclastic floatstones may be hardgrounds that record a break in sedimentation during which seafloor lithification occurred. If these intervals are hardgrounds, the tops of unlithified lithoclastic floatstones can be interpreted to represent flooding surfaces, and thus the bases of higher order sequence stratigraphic cycles.

On the other hand, several features suggest that lithoclasts may have been transported. Lithoclasts are often rounded, and completely encrusted by bryozoans and serpulid worm tubes (Fig. 10). In addition, observation of skeletal grains within lithoclasts suggests that lithoclasts were derived upslope from older sediments. If lithoclasts represent transported material, then unlithified lithoclastic floatstones can be interpreted to represent transgressive lag deposits, and the bases of these intervals to represent the bases or lowstand deposits of high-frequency sea-level changes.

Recovery of Unit II sediments was relatively poor at both Sites 1008 and 1009. At Site 1009, recovered Unit II sediments consist of an apparently unordered succession of partially lithified bioclastic mudstones, partially lithified bioclastic mudstones to wackestones, partially lithified bioclastic wackestones, and partially lithified lithoclastic floatstones. Recovery of Unit II sediments at Site 1008 was too poor to characterize the sedimentary succession, or to allow for direct comparison with Unit II sediments recovered at Site 1009. However, both sites are marked by an interval of no recovery that occurs just below an interval of unlithified lithoclastic floatstone (Cores 166-1008A-12X through 14X; Core 166-1009A-21X). These unlithified lithoclastic floatstones show reverse grading and an upward increase in grain size and grain abundance, and are interpreted to represent debris flows.

BIOSTRATIGRAPHY

Expanded sections of Pleistocene sediments were recovered at Sites 1008 and 1009. The nannofossil biostratigraphy indicates the presence of Zones NN19 through NN21, whereas the planktonic foraminiferal biostratigraphy is restricted to Zone N22. Upper Pliocene faunas and floras were found in the lower part of the sections, indicating substantial reworking.

Calcareous Nannofossils

Site 1008

Thirteen samples from Hole 1008A were examined for the distribution of age-diagnostic calcareous nannofossil species. Calcareous nannofossil datum levels are listed in Table 2 and shown in Figure 12. Calcareous nannofossils from this hole are moderately to poorly preserved. The bottom sample from this hole was barren of nannofossils.

The first occurrence of *Emiliania huxleyi*, which defines the NN21/20 boundary (0.25 Ma), is placed between Samples 166-

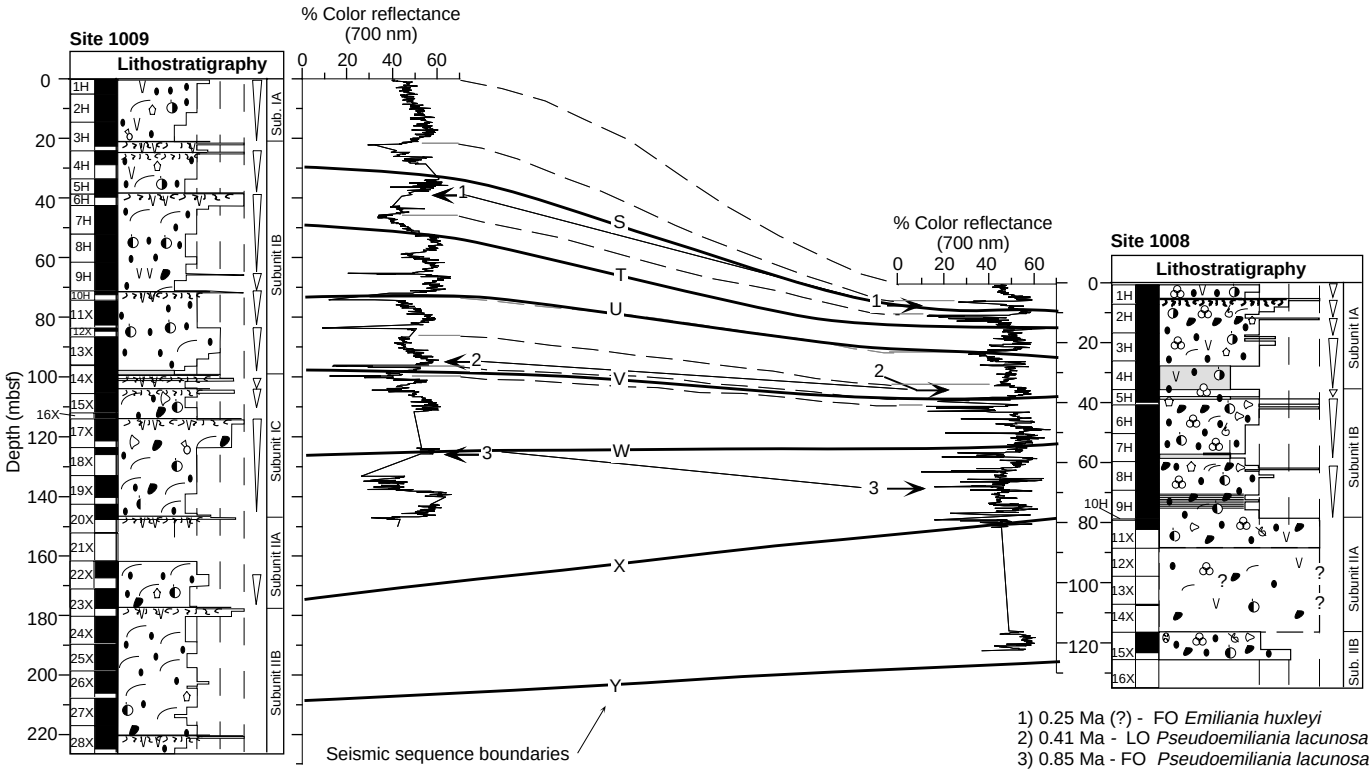

Figure 11. Correlation of Sites 1008 and 1009 on the basis of lithology, color reflectance data, seismic sequence boundaries, and calcareous nannofossil data.

Table 2. Calcareous nannofossil bioevents at Sites 1008/1009.

Event	Age (Ma)	Interval (cm)	Depth* (mbsf)
Site 1008			
B *E. huxleyi* (NN20/21)	0.25	1008A-1H-CC to 1008A-2H-CC	11.33
T *P. lacunosa* (NN19/20)	0.41	1008A-4H-CC to 1008A-5H-CC	37.13
T *R. asanoi*	0.85	1008A-8H-CC to 1008A-9H-CC	73.30
Site 1009			
B *E. huxleyi* (NN20/21)	0.25	1009A-6H-CC to 1009A-7H-CC	45.51
T *P. lacunosa* (NN19/20)	0.41	1009A-13H-CC to 1009A-14H-CC	101.82
T *R. asanoi*	0.85	1009A-18X-CC to 1009A-19X-CC	132.91
B *R. asanoi*	1.16	1009A-20X-CC to 1009A-21X-CC	149.75
T *Gephyrocapsa* spp. (large)	1.20	1009A-22X-CC to 1009A-23X-CC	172.23
B *Gephyrocapsa* spp. (large)	1.44	1009A-28X-CC	224.53

Notes: B = base, T = top. * = average depth for the interval; for actual interval depth, see coring summary on CD-ROM. Average depth was used for constructing Figure 12.

1008A-1H-CC and 2H-CC (11 mbsf). The top of *Pseudoemiliania lacunosa* was found in Sample 166-1008A-5H-CC, which defines the base of Zone NN20 (0.41 Ma). *P. lacunosa, Gephyrocapsa caribbeanica,* and *Gephyrocapsa oceanica* are present in Samples 166-1008A-5H-CC through 14X-CC, and this interval can be assigned to Zone NN19. Within this section, the first occurrence of *Gephyrocapsa parallela* (just above the Jaramillo Event; 0.95 Ma) is detected between Samples 166-1008A-8H-CC and 9H-CC). *Reticulofenestra asanoi,* which ranges from 0.85 to 1.16 Ma, occurs in Samples 166-1008A-9H-CC and 11X-CC. Sample 166-1008A-14X-CC contains large-form *Gephyrocapsa* (larger than 6 µm), which indicates that this sample has an age range of 1.20 to 1.44 Ma.

Site 1009

Twenty-nine samples from Hole 1009A were examined for age-diagnostic calcareous nannofossils. Nannofossil datum levels are listed in Table 2 and shown in Figure 12. Calcareous nannofossils from this hole in general are moderately preserved. Nannofossils in the lowermost eight samples are poorly preserved.

E. huxleyi, the first occurrence of which defines the NN21/20 boundary (0.25 Ma), was found in Samples 166-1009A-1H-CC through 6H-CC. *P. lacunosa,* the last occurrence of which defines the base of Zone NN20, was found in Samples 166-1009A-14H-CC through 28X-CC (total depth). *G. caribbeanica* was found throughout Hole 1009A, which indicates that the entire recovered sequence can be assigned to the Pleistocene. *G. caribbeanica* co-occurs with *G. oceanica* throughout the section in this hole. The nannofossil distribution indicates that the intervals from the top through Sample 166-1009A-6H-CC (0–46 mbsf), Samples 7H-CC through 13H-CC (46–102 mbsf), and Samples 14H-CC through 28X-CC (102–225 mbsf) correspond to the Pleistocene Zones NN21, NN20, and NN19, respectively.

The first occurrence of *G. parallela* (just above the Jaramillo Event; 0.95 Ma) is detected between Samples 166-1009A-18X-CC and 19X-CC. *R. asanoi,* which ranges between 0.85 and 1.16 Ma, occurs in Sample 166-1009A-20X-CC. Samples 166-1009A-23X-CC through 28X-CC (total depth) contain large-form *Gephyrocapsa* (larger than 6 µm), which indicates that this section is between 1.20 and 1.44 Ma old.

Planktonic Foraminifers

Sites 1008 and 1009

Planktonic foraminifers recovered from Sites 1008 and 1009 are generally rare to common and preservation is very good in the upper parts of Holes 1008A and 1009A. In Samples 166-1009A-1H-CC through 3H-CC, planktonic foraminiferal tests are transparent and seem to indicate a Holocene age. In the lower sections of both holes, planktonic foraminifers are common to abundant, but preservation has deteriorated significantly with many specimens completely recrystallized, discolored, or phosphatized. The presence of *Globorotalia truncatulinoides* in the lowermost samples at Holes 1008A and 1009A indicates that the recovered sediments from both sites are assigned to Zone N22. Reworking occurs throughout the lower intervals. Species from Zones N20 and N21, including *Globigerinoides extremus, Globigerinoides fistulosis, Globorotalia miocenica,* and *Globorotalia limbata*, were found in Samples 166-1008A-7H-CC through 15X-CC and Samples 166-1009A-12H-CC through 28X-CC.

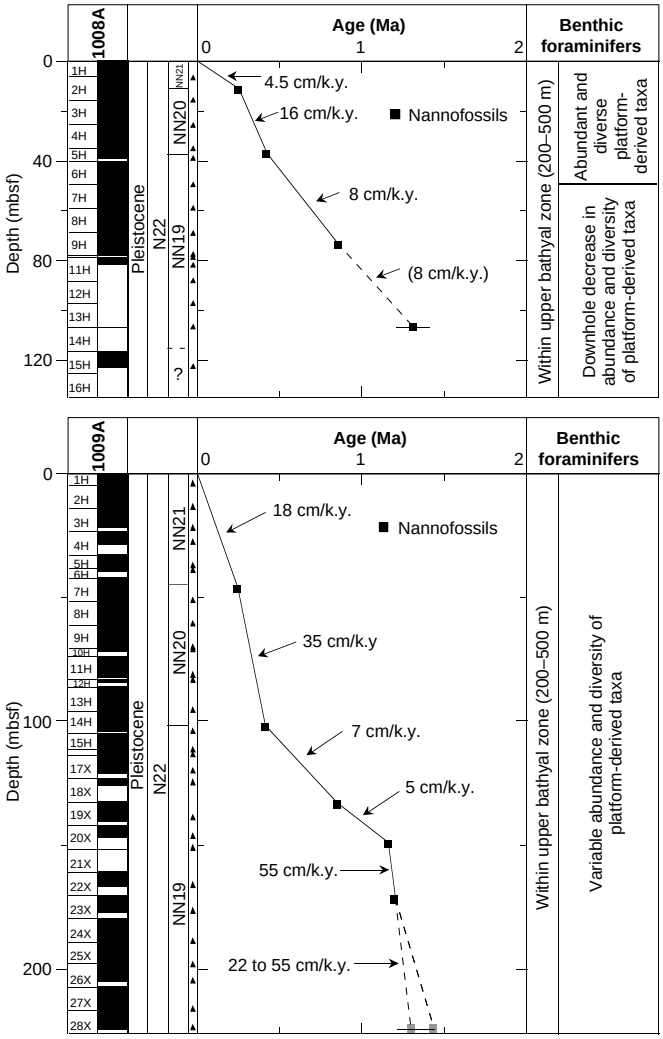

Figure 12. Calcareous nannofossil and planktonic foraminiferal zonation and benthic foraminiferal faunal changes for Sites 1008/1009. Recovery for the holes at each site is adjacent to the cores. Solid triangles mark the position of samples examined for stratigraphy and benthic foraminiferal faunas. The age-depth plots are based on the biohorizons in Table 2.

Benthic Foraminifers

Site 1008

Hole 1008A yields benthic foraminiferal faunas that contain *Bulimina marginata* (~30–600 m), *Cibicidoides incrassatus* (~100–600 m), *Cibicidoides mundulus* (>600 m), *Planulina foveolata* (~100–500 m), *Planulina ariminensis* (~100–800 m), and *Sigmoilopsis schlumbergeri* (>200 m) (van Morkhoven et al., 1986), indicating a paleodepth of ~200–500 m (within the upper bathyal zone). Other

common taxa typical of the upper bathyal assemblages in this section are similar to those found at Sites 1003, 1004, and 1005 (see "Biostratigraphy" section, "Site 1003" chapter, this volume). Hole 1008A also contains abundant platform-derived shallow-water taxa similar to those found at Sites 1003, 1004, and 1005 (see "Biostratigraphy" section, "Site 1003" chapter, this volume), with diversity and abundance decreasing below Core 166-1008A-6H.

Site 1009

Hole 1009A yields benthic foraminiferal faunas that contain *B. marginata* (~30–600 m), *C. incrassatus* (~100–600 m), *C. mundulus* (>600 m), *P. foveolata* (~100–500 m), *P. ariminensis* (~100–800 m), and *S. schlumbergeri* (>200 m) (van Morkhoven et al., 1986), indicating a paleodepth of ~200–500 m (within the upper bathyal zone). Other common taxa typical of the upper bathyal assemblages in this section are similar to those found at Sites 1003, 1004, 1005, and 1008 (see "Biostratigraphy" section, "Site 1003" chapter, this volume). Hole 1009A also contains abundant platform-derived shallow-water taxa similar to Sites 1003, 1004, 1005, and 1008 (see "Biostratigraphy" section, "Site 1003" chapter, this volume). The diversity and abundance of transported taxa are extremely variable among samples, ranging from approximately 20% to 70%. Preservation of benthic foraminifers is also highly variable.

Sedimentation Rates

Site 1008

An expanded Pleistocene sequence was recovered at Site 1008. Four nannofossil datum levels were recognized and used to construct an age vs. depth plot for this site (Fig. 12). Individual datums are listed in Table 2. The sedimentation rate is variable throughout the sequence. The base of nannofossil Zone NN21 (0.25 Ma) occurs between Samples 166-1008A-1H-CC and 2H-CC (6.6 to 16.1 mbsf). The sedimentation rate is 4.5 cm/k.y., taking the midpoint of the interval as the NN20/21 boundary. The sedimentation rate increases to 6.5 cm/k.y. if this boundary is placed just above Sample 166-1008A-2H-CC. Within this upper zone, the planktonic foraminifers in Sample 166-1008A-1H-3, 0–5 cm, (3 mbsf) are very rare and almost transparent, indicating that they may be assigned to the Holocene. If true, then this would require sedimentation rates on the order of 30 to 50 cm/k.y. in the upper 3 m of Hole 1008A. This also illustrates that within the individual intervals defined by the nannofossil events that there is significant variability in sedimentation.

The interval including Samples 166-1008A-2H-CC through 4H-CC (11–37 mbsf) is characterized by higher sedimentation rates (16 cm/k.y.). Placing the NN20/21 boundary just above Sample 166-1008A-2H-CC decreases the rate to 13 cm/k.y.

The interval defined by Zone NN19 shows a sedimentation rate of 8 cm/k.y. The lowermost sample examined in this hole, Sample 166-1008A-14X-CC (107 mbsf), is between 1.2 and 1.44 Ma in age. If the midpoint of this age range is taken for Sample 166-1008A-14X-CC, then the sedimentation rate is 8 cm/k.y., which is the same as the upper part of Zone NN19.

Site 1009

The three Pleistocene nannofossil zones found at Site 1009 span about 1.4 m.y. Six nannofossil datum levels were recognized and used to construct an age vs. depth plot for this site (Fig. 12). Individual datums are listed in Table 2.

The uppermost nannofossil Zones NN21 (0–0.25 Ma) and NN20 (0.25–0.41 Ma) have sedimentation rates of 18 cm/k.y.and 35 cm/k.y., respectively. In Cores 166-1009A-1H through 3H planktonic foraminifers are very rare and transparent, indicating that these are Holocene deposits. In this case, the sedimentation rate would be greater than 300 cm/k.y. for the upper 23 m. The interval from 100 to 150 mbsf is in the upper part of Zone NN19 (0.41–1.16 Ma) and has a sedimentation rate between 5 and 7 cm/k.y. Below this interval, the sedimentation rate is substantially increased in the lower part of Zone NN19. Sample 166-1009A-28X-CC is still Pleistocene in age and younger than 1.44 Ma. If this is considered the base of the large *Gephyrocapsa* spp., then the sedimentation rate is 22 cm/k.y. However, it would be substantially higher if this represented the middle of the large *Gephyrocapsa* spp. range (1.2–1.44 Ma). In this case, the sedimentation rate would be 55 cm/k.y.

PALEOMAGNETISM

Hole 1008A

Shipboard paleomagnetic measurements were conducted at Hole 1008A on the archive-half of APC cores at 10-cm intervals to a depth of 76.15 mbsf. Measurements, using a whole-core cryogenic magnetometer with in-line AF demagnetizer, were taken of the natural remanent magnetization (NRM). The NRM values ranged from 19.83 to 0.09 mA/m, with an average intensity of 0.24 mA/m (Fig. 13). However, 97% of the NRM measurements passed a Z:X ratio reliability criteria of greater than or equal to 0.7 (for definition, see "Paleomagnetism" section, "Explanatory Notes" chapter). The NRM record shows a series of fluctuations similar to the magnetic susceptibility record (see below) and may represent intervals during which magnetic mineral preservation varied.

A demagnetization step of 15 mT was applied to Cores 166-1008A-1H through 3H. This typically reduced the NRM intensity by 62%, with intensity values varying from 4.46 to 0.044 mA/m (average NRM intensity = 0.801 mA/m). Seventy-six percent of the measurements after the 15-mT AF demagnetization step passed the Z:X ratio reliability criteria (≥0.7).

The magnetic susceptibility (MS) record for Hole 1008A was measured on the whole-core MST at 10-cm intervals; it revealed a signal that was dominantly diamagnetic, but fluctuated between a minimum negative value of –4.3 and a maximum positive value of 4.2 (Fig. 13). Eighty-two percent of the measurements indicated diamagnetic behavior.

Saturation isothermal remanent magnetization (SIRM) acquisition tests were conducted on individual samples from the working half of Cores 166-1008A-2H and 3H (i.e., on 2H-1, 91–93 cm; 2H-5, 94–96 cm; 3H-3, 125–127 cm; 3H-6, 95–97 cm; and 3H-7, 47–49 cm) and indicate that the remanence is carried by single-domain magnetite with admixtures of hematite (Fig. 14). Moreover, variations in grain size and the composition of single-domain magnetite occur

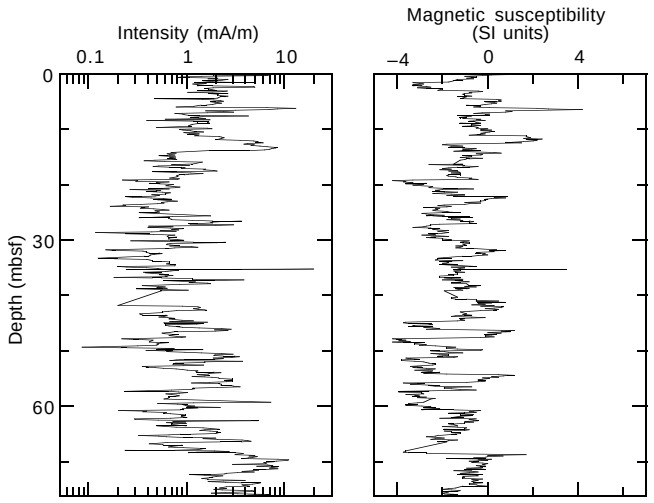

Figure 13. Archive-half NRM intensity and whole-core magnetic susceptibility for the interval from 0 to 76.15 mbsf in Hole 1008A.

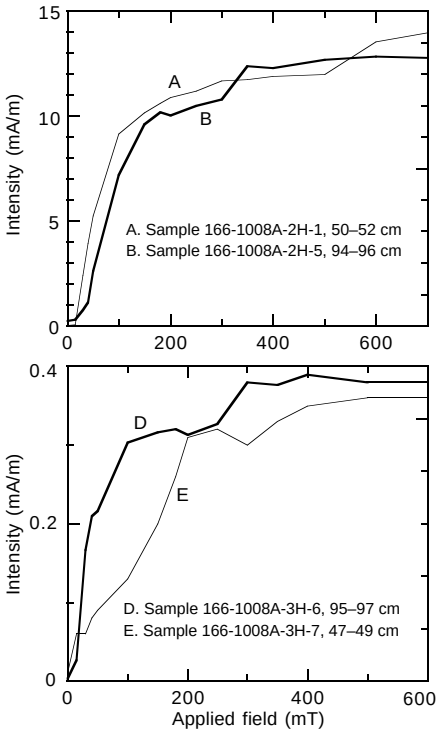

Figure 14. Plots of SIRM experiments on discrete samples from the working half of Cores 166-1008A-2H and 3H. Samples 166-1008A-2H-5, 94–96 cm, and 3H-6, 95–97 cm, appear to contain magnetite with admixtures of hematite.

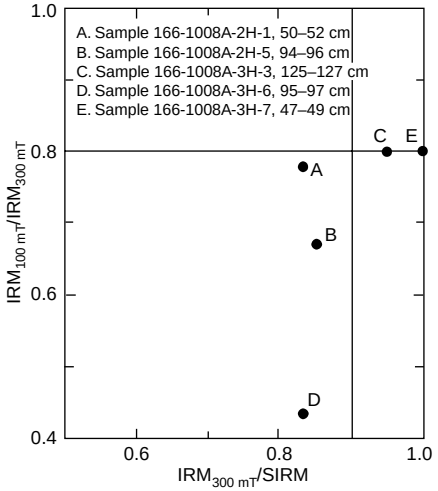

Figure 15. Plot of $IRM_{300\ mT}/SIRM$ vs. $IRM_{100\ mT}/IRM_{300\ mT}$ for samples taken from the working half of Cores 166-1008A-2H and 3H (A = unlithified packstone-wackestone; B = unlithified foraminifer peloid wackestone; C = partially lithified packstone-wackestone; D = unlithified foraminifer wackestone; and E = unlithified peloidal wackestone). The data are less well grouped than at previous sites, but plot close to the single-domain magnetite region of the plot. This suggests variation in grain size and composition.

throughout the samples (Fig. 15). Apart from Sample 166-1008A-2H-1, 50–52 cm, which had an MS value of zero, the samples collected for the SIRM experiments possess negative MS values. This indicates that variations in magnetic mineralogy are not responsible for fluctuations in the susceptibility profile at Hole 1008A. Instead, these variations are most likely a product of magnetic mineral concentrations and are governed, therefore, by preservation or input processes. Magnetic susceptibility fluctuations appear to correlate with variations in NRM intensity (Fig. 13), with low NRM intensity correlating with more strongly diamagnetic behavior.

Variations in magnetic inclination during demagnetization of Cores 166-1008A-2H through 3H have enabled the tentative definition of a polarity event at Hole 1008A (Fig. 16). Inclination values from Cores 166-1008A-1H and 3H, before demagnetization, ranged from 85° to –26°, with an average value of 56°. Less than 0.01% of the NRM values possessed negative inclinations, indicating a dominantly normal polarity NRM component. Demagnetization at 15 mT caused a reduction in inclination of approximately 31°, with an increase in negative inclination (0.06%). Between 0 and 18.95 mbsf, positive magnetic inclination was observed, suggesting an interval of normal polarity. However, a series of short polarity reversals, defined by single measurement points of negative magnetic inclination, were observed at 0.95, 3.25, 4.45, and 12.85 mbsf. Fifty percent of the negative inclination values was located between 15.65 and 16.15 mbsf, defining a 0.5-m-thick interval of reversed inclination. Application of a Z:X ratio-based reliability threshold for directional data (>0.7) failed to affect the thickness of this polarity event. Below this zone, magnetic inclination was positive, implying normal polarity (Brunhes). Further polarity determination was not attempted in Hole 1008A because magnetic intensity was too low.

The proposed reversal/excursion has been correlated with the Blake Event (0.13 Ma), based upon the first occurrence of the nannofossil *Emiliania huxleyi*, which appears at 16.08 mbsf (0.25 Ma) in Sample 166-1008A-2H-CC. However, the polarity reversal/excursion that immediately overlies this biostratigraphic datum suggests a hiatus or local variation in the first occurrence of *E. huxleyi.*

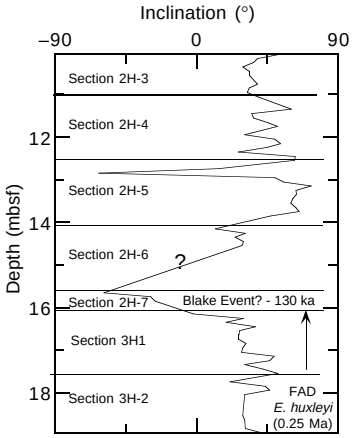

Figure 16. Plot of magnetic inclination against depth in Sections 166-1008A-2H-3 to 3H-2. A reversed polarity event can be defined on the basis of variations in inclination. No declination control exists. Application of a Z:X ratio-based reliability threshold for directional data has been applied. This polarity event has been correlated with the Blake Event, based on the first occurrence of the nannofossil *Emiliania huxleyi.*

Hole 1009A

Shipboard paleomagnetic measurements were conducted at Hole 1009A on the archive-half of APC cores at 10-cm intervals to a depth of 111.8 mbsf. No shipboard magnetostratigraphy was developed from the paleomagnetic data. Measurements, using a whole-core cryogenic magnetometer with in-line AF demagnetizer, were made of the NRM. The NRM values ranged from 26.79 to 0.11 mA/m, with an average intensity of 3.63 mA/m (Fig. 17). The NRM record shows several subtle trends in intensity; most striking are the lower values in the top 5 m of the core. Several zones of higher intensity (>5 mA/m)

were present in the APC cores, although some of the very high intensity spikes (up to 2802 mA/m) are attributed to coring contamination (i.e., at approximately 73 and 96 mbsf).

SIRM acquisition tests were conducted on individual samples from the working half of Cores 166-1009A-7H, 9H, and 11H and indicate (along with a diamagnetic susceptibility) that the remanence is carried by single-domain magnetite (Fig. 18). This uniform single-domain magnetite mineralogy is considerably different from the mixed magnetite/hematite mineralogy suggested from shipboard SIRM measurements at Hole 1008A.

The magnetic susceptibility record for Hole 1009A was measured on the whole-core MST at 10-cm intervals. The susceptibility data were mostly diamagnetic (88.3%) and fluctuated between a minimum negative value of −6.6 and a maximum positive value of 15.2 (Fig. 19).

Magnetic inclination variations at the NRM level did not allow any correlation to the GPTS. Several 20- to 30-cm-thick intervals of reverse polarity were present in the whole-core data and in at least two cases correlated with drilling disturbed intervals (that is, at 73 and 96 mbsf).

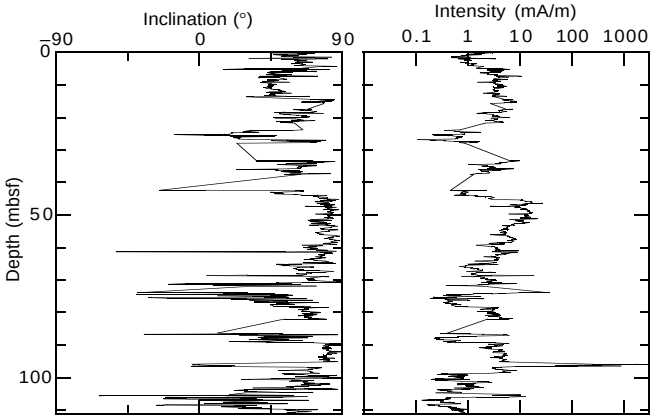

Figure 17. NRM inclination and intensity from APC cores at Site 1009.

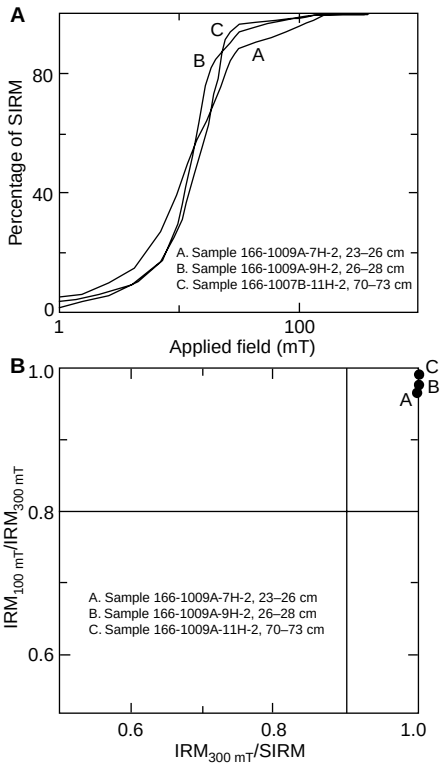

Figure 18. **A.** Plots of SIRM measurements on discrete samples from Hole 1009A. **B.** Plot of $IRM_{300\ mT}$/SIRM vs. $IRM_{100\ mT}/IRM_{300\ mT}$ for samples taken from the working half of cores from Hole 1009A. The saturation pattern is characteristic of a single-domain magnetite remanence carrier.

ORGANIC GEOCHEMISTRY

At Sites 1008 and 1009, the shipboard organic geochemistry program included determinations of inorganic carbon, total carbon, total nitrogen, and total sulfur, in addition to safety monitoring for hydrocarbon gases. The analytical procedures are described in the "Explanatory Notes" chapter, this volume.

Volatile Hydrocarbons

At Site 1008, low methane (C_1) concentrations (3–5 ppm) were observed between 0 and 57.2 mbsf. Below this depth, methane increases from 9 to 174 ppm at 120.6 mbsf (Table 3 on CD-ROM; Fig. 20). Trace levels of ethane (C_2) (<1 ppm) were detected at 76.2 mbsf and the C_1/C_2 decreased from 36 at 76.2 mbsf to 22 at 120.6 mbsf (Table 3 on CD-ROM). Trace levels of propane and isopentane were detected at 120.6 mbsf together with small quantities (41 ppm) of hydrogen sulfide (H_2S) at the base of the section (120.6 mbsf) (Table 3 on CD-ROM).

At Site 1009, methane concentrations show a steady increase from 3 ppm at 1.5 mbsf to 352 ppm at 78.3 mbsf (Table 4 on CD-ROM; Fig. 21). Below this depth, methane concentrations remain stable near 300 ppm. Ethane was first detected at 49.8 mbsf, and the C_1/C_2 decreases from approximately 100 at 49.8 mbsf to 39 at 222.7 mbsf (Fig. 21). Trace levels of heavy-weight hydrocarbons were observed below 145.2 mbsf (Table 4 on CD-ROM). Hydrogen sulfide is present at low levels from 26.8 to 64.3 mbsf (22–72 ppm). At 78.3 mbsf, hydrogen sulfide concentrations increase to 5075 ppm, after which sulfide concentrations stabilize to approximately 8000 ppm (Fig. 21).

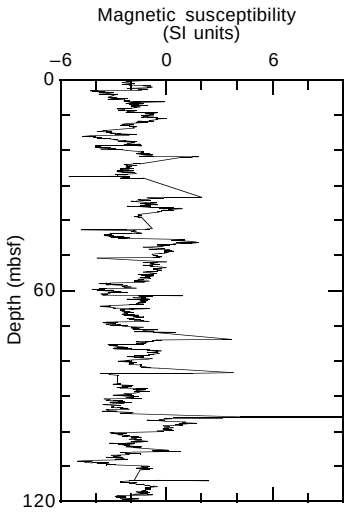

Figure 19. Summary of whole-core magnetic susceptibility data from Hole 1009A. The predominantly diamagnetic signal reflects the high carbonate and mainly single-domain magnetite remanence.

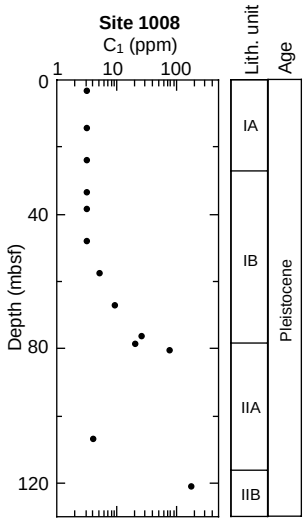

Figure 20. Concentration of methane (C_1) of headspace gases at Site 1008.

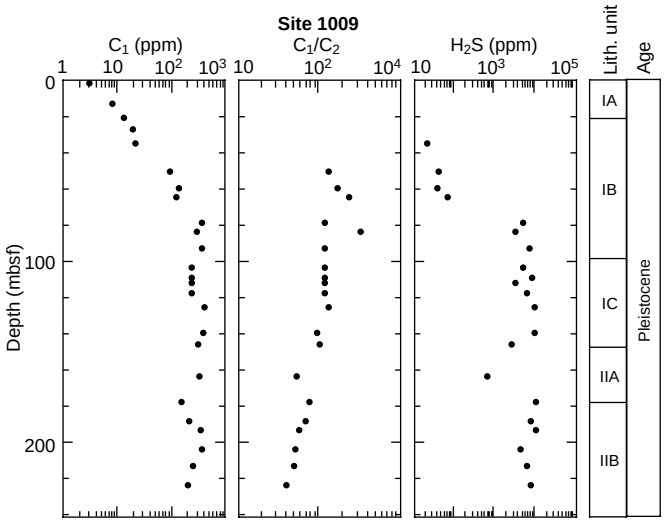

Figure 21. Concentration of methane (C_1), methane/ethane (C_1/C_2), and hydrogen sulfide (H_2S) of headspace gases at Site 1009.

Inorganic and Organic Carbon, Total Sulfur, and Total Nitrogen

Carbonate data for Sites 1008 and 1009 are presented in Figure 22 and in Tables 5 and 6 on CD-ROM. Six samples from Site 1008 and 12 samples from Site 1009 with low carbonate content were selected for total organic carbon (TOC), total nitrogen (TN), and total sulfur (TS) analysis.

At Site 1008, carbonate content varies from 91.5 to 96.8 wt%. Within lithologic Unit I, a general increase in carbonate content was observed from 92 to 95 wt% (Fig. 22). The TOC varied between 0.1 and 0.5 wt%. Highest TOC contents (>0.5 wt%) were measured within lithologic Subunits IA and IIB (22.5 and 122.5 mbsf). TS varies between 0.04 and 0.24 wt% (Table 5 on CD-ROM). TN concentrations are low (0.00–0.15 wt%), generally below the detection limit (<0.1 wt%) (Table 5 on CD-ROM).

At Site 1009, the carbonate content varies between 91.5 and 96.9 wt% (Table 6 on CD-ROM; Fig. 22). There is a general increase in carbonate content through lithologic Unit I, and overall there is a higher variation than at Site 1008. At Site 1009, lithologic Subunit IIA exhibits large changes in carbonate content compared with Subunit IIB. TOC contents vary from 0.0 to 1.92 wt%, with the highest values (>0.5 wt%) found within all lithologic units except Subunit IIB (Table 6 on CD-ROM). The TS concentrations vary between 0.00 and 0.27 wt% (Table 6 on CD-ROM). The TN concentrations are low (0.05–0.1 wt%) and generally below detection limits (<0.1 wt%) (Table 6 on CD-ROM).

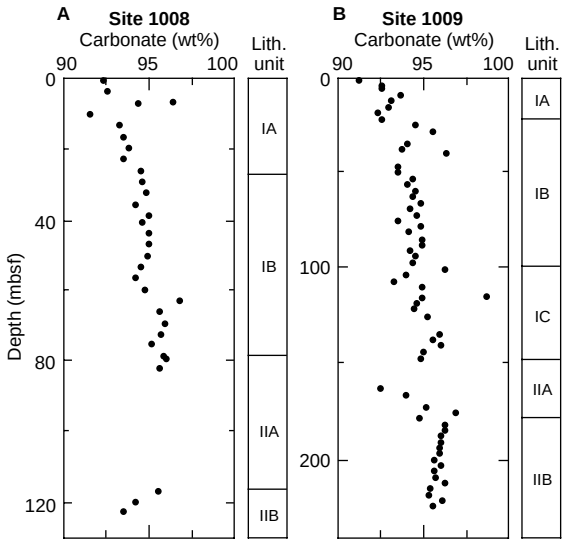

Figure 22. Carbonate contents from Sites 1008/1009.

Discussion

The headspace gas composition varies considerably between Sites 1008 and 1009. At Site 1009, methane concentrations increase just below seafloor, whereas at Site 1008 the methane concentrations increase below 47.7 mbsf. Overall, the methane and hydrogen sulfide concentrations are higher at Site 1009 than at Site 1008. The depletion of sulfate in the pore water is also greater at Site 1009 than at Site 1008; although total depletion of sulfate was not observed at either of the sites (see "Inorganic Geochemistry" section, this chapter). The increase in H_2S concentrations below 60.3 mbsf at Site 1009 coincides with a reduction in the interstitial SO_4^{2-} concentration. The most likely explanation for this relationship is that in situ organic matter is being oxidated by sulfate reducing bacteria (see "Inorganic Geochemistry" section, this chapter). The slightly higher TOC contents of Site 1009 relative to Site 1008 support this conclusion.

The generally low C_1/C_2 observed at both sites probably results from the preferential loss of C_1 by either diffusion or selective microbiological C_1 consumption (Claypool and Kvenvolden, 1983). The presence of trace levels of higher weight hydrocarbons in the headspace gases below 145.5 mbsf at Site 1009 indicates that nonbiological decomposition of organic matter may also contribute to some of the gas composition at Site 1009.

INORGANIC GEOCHEMISTRY

Inorganic chemical analyses were conducted on 46 interstitial water samples collected at Sites 1008 and 1009. Two whole-round samples were taken from each of the first six cores at Site 1008 and from each of the first nine cores at Site 1009, and one whole-round sample was collected per core thereafter in both holes. Analytical methods are detailed in the "Inorganic Geochemistry" section of the "Explanatory Notes" chapter, this volume. Interstitial water analytical data

Table 7. Composition of interstitial waters from Sites 1008/1009.

Core, section, interval (cm)	Depth (mbsf)	pmH	pH	Alkalinity (mM)	Salinity	Cl^- (mM)	Na^+ (mM)	Mg^{2+} (mM)	Ca^{2+} (mM)	SO_4^{2-} (mM)	HPO_4^{2-} (µM)	NH_4^+ (µM)	H_4SiO_4 (µM)	K^+ (mM)	Li^+ (µM)	Fe^{2+} (µM)	Sr^{2+} (µM)	F^- (µM)
166-1008A-																		
1H-2, 145–150	3	7.71	7.71	2.8	36.5	574	495	56.3	11.5	29.9	3.9	46	29	11.3	28	4	110	85
1H-4, 145–150	6	7.57	7.57	2.5	36.5	574	493	56.6	11.0	29.5	1.8	66	44	11.5	30	3	99	80
2H-3, 140–150	11	7.52	7.56	2.3	36.5	572	503	57.4	11.2	29.5	1.5	58	38	11.1	31	4	109	85
2H-5, 140–150	14	7.52	7.72	2.4	36.5	571	486	56.5	10.9	29.4	1.8	113	55	11.1	29	4	115	96
3H-3, 140–150	21	5.75	7.66	2.7	36.5	573	506	56.6	10.9	29.7	5.7	119	71	11.4	29	4	122	100
3H-5, 140–150	24	7.61	7.76	2.7	36.5	574	512	57.2	11.4	29.9	0.9	107	31	10.8	30	5	117	100
4H-2, 140–150	29	7.61	7.80	2.2	36.5	573	496	56.7	11.0	29.6	0.9	109	34	10.9	32	5		103
4H-5, 140–150	33	7.54	7.74	2.8	36.5	573	510	58.1	11.2	29.9	1.2	119	31	10.9	29	5	122	104
5H-2, 140–150	38	7.52	7.74	2.6	36.5	574	503	57.1	10.8	30.1	1.5	133	36	11.1	30	7	124	100
6H-2, 140–150	43	7.42	7.74	3.0	36.5	577	505	57.5	11.9	30.1	1.5	175	47	11.6	31	6	146	110
6H-5, 140–150	48	7.39	7.89	3.2	37.0	578	505	56.1	10.8	29.7	1.2	240	55	11.3	30	5	176	128
7H-5, 140–150	57	7.32	7.82	4.0	37.0	580	504	56.3	11.3	30.0	0.9	400	84	11.1	35	6	255	196
8H-5, 140–150	67	6.98	7.81	9.4	37.5	590	526	57.4	10.4	28.3	2.7	934	110	12.0	41	6	455	297
9H-5, 140–150	76	6.76	7.95	13.8	37.5	600	526	55.7	9.9	26.2	2.4	1380	149	11.5	46	14	606	339
11X-1, 140–150	80	6.92	8.08	15.9	38.0	615	528	54.2	9.6	23.2	3.0	1665	157	11.8	48	2	700	362
15X-3, 140–150	121	6.56	6.99	32.8	40.0	653	559	43.0	8.0	13.2	3.9	4106	246	12.7	64	3	1057	392
166-1009A-																		
1H-1, 140–150	1	7.78	7.87	3.1	37.0	579	507	58.0	11.5	29.6	1.5	54	14	11.9	28	4	97	77
1H-3, 137–147	4		7.93	3.3	37.0	580	492	54.9	10.8	30.1	0.9	165	23	10.8	28	10	100	80
2H-2, 140–150	8		7.92	3.8	37.0	580	503	57.1	11.0	30.5	1.5	211	36	11.8	30	7	101	80
2H-5, 140–150	12	7.10	8.05	8.5	37.0	578	512	57.7	10.6	27.4	3.9	819	81	10.8	30	7	99	83
3H-2, 140–150	17		8.15	9.0	37.0	582	497	57.0	10.1	26.0	4.2	1047	94	11.7	31	11	108	88
3H-4, 140–150	20	7.12	8.07	7.6	36.5	579	499	57.8	9.8	26.7	3.6	1016	79	10.8	32	5	99	86
4H-2, 140–150	27		8.10	5.2	37.5	580	507	57.9	11.6	28.3	1.8	529	47	11.8	34	8	109	86
5H-1, 140–150	35	7.14	8.10	6.8	37.5	588	510	57.1	11.4	28.1	2.7	668	60	11.6	35	6	109	84
5H-3, 148–158	38		8.28	7.3	37.5	596	514	57.0	10.8	26.9	3.0	668	66	11.1	38		118	88
7H-2, 140–150	45		7.38	13.9	39.0	611	523	56.5	11.0	24.7	3.3	1951	71	12.1	38	5	115	89
7H-5, 140–150	50	6.80	7.87	15.5	39.5	619	542	56.6	10.8	23.3	5.1	1862	77	13.1	39	7	116	95
8H-2, 140–150	55		8.02	17.5	40.0	630	545	55.9	10.8	22.0	6.0	2575	88	11.5	40	6	123	93
8H-5, 140–150	59	6.61	7.98	21.4	40.0	635	533	55.1	11.3	20.5	5.7	2539	94	12.5	38	6	143	99
9H-2, 140–150	64		8.02	24.1	40.5	637	542	54.1	10.1	18.3	7.5	3287	99	13.3	40	7	166	113
9H-5, 140–150	69	6.49	8.13	27.2	41.0	664	551	53.9	10.1	14.9	5.7	3946	103	13.1	41	5	163	122
11H-3, 135–150	78	6.59	8.15	30.8	42.0	679	563	54.3	10.3	13.7	5.1	4517	94	13.0	39	6	227	131
13H-6, 135–150	95	6.46	8.21	30.6	44.0	704	588	57.5	10.4	16.7	3.0	4249	86	14.1	43	6	470	185
14H-5, 135–150	103	6.44	8.18	30.9	45.0	717	593	57.7	11.7	18.0	5.7	4321	144	14.9	50	17	745	305
15H-2, 135–150	108	6.46	7.24	33.1	46.0	726	599	57.3	12.4	18.2	3.9	4517	177	14.7	49	7	856	351
17X-4, 135–150	120	6.44	6.83	31.6	46.0	726	623	60.1	13.2	19.0	4.5	4837	214	14.0	54	9	908	354
18X-1, 135–150	124	6.51	7.45	32.1	45.5	729	602	59.0	11.1	18.6	4.8	4356	218	14.6	57	8	911	354
19X-4, 135–150	139	6.44	7.87	33.0	45.5	730	603	60.7	10.3	18.1	4.5	4873	225	13.4	56	4	948	309
20X-2, 135–150	145	6.51	7.00	33.3	45.5	725	605	60.1	10.6	18.2	5.4	5140	214	14.4	59	13	855	280
22X-1, 135–150	163	6.71	7.12	31.7	45.0	717	597	56.3	9.6	16.0	6.0	5318	197	13.9	58	7	861	275
23X-4, 135–150	177	6.37	7.12	34.5	44.0	708	594	53.7	10.1	14.3	4.2	4802	223	13.7	65	2	1073	316
24X-5, 135–150	188	6.44	7.84	34.3	44.0	705	588	51.9	10.6	13.6	3.9	5283	251	13.7	68	10	1307	360
25X-2, 135–150	192	6.53	7.56	33.8	44.0	703	586	50.9	10.4	13.4	4.2	5639	264	13.8	67	9	1302	367
26X-4, 135–150	204		7.79	34.9	43.5	699	588	49.9	10.6	13.2	2.7	5710	299	13.6	70	7	1354	370
27X-3, 135–150	212		7.96	35.2	43.0	697	579	48.8	10.5	12.2	6.9	5479	309	13.0	70	6	1417	364
28X-4, 135–150	223	6.59	7.37	35.7	42.5	696	583	47.6	10.4	11.9	6.3	3822	327	13.1	73	3	1433	373

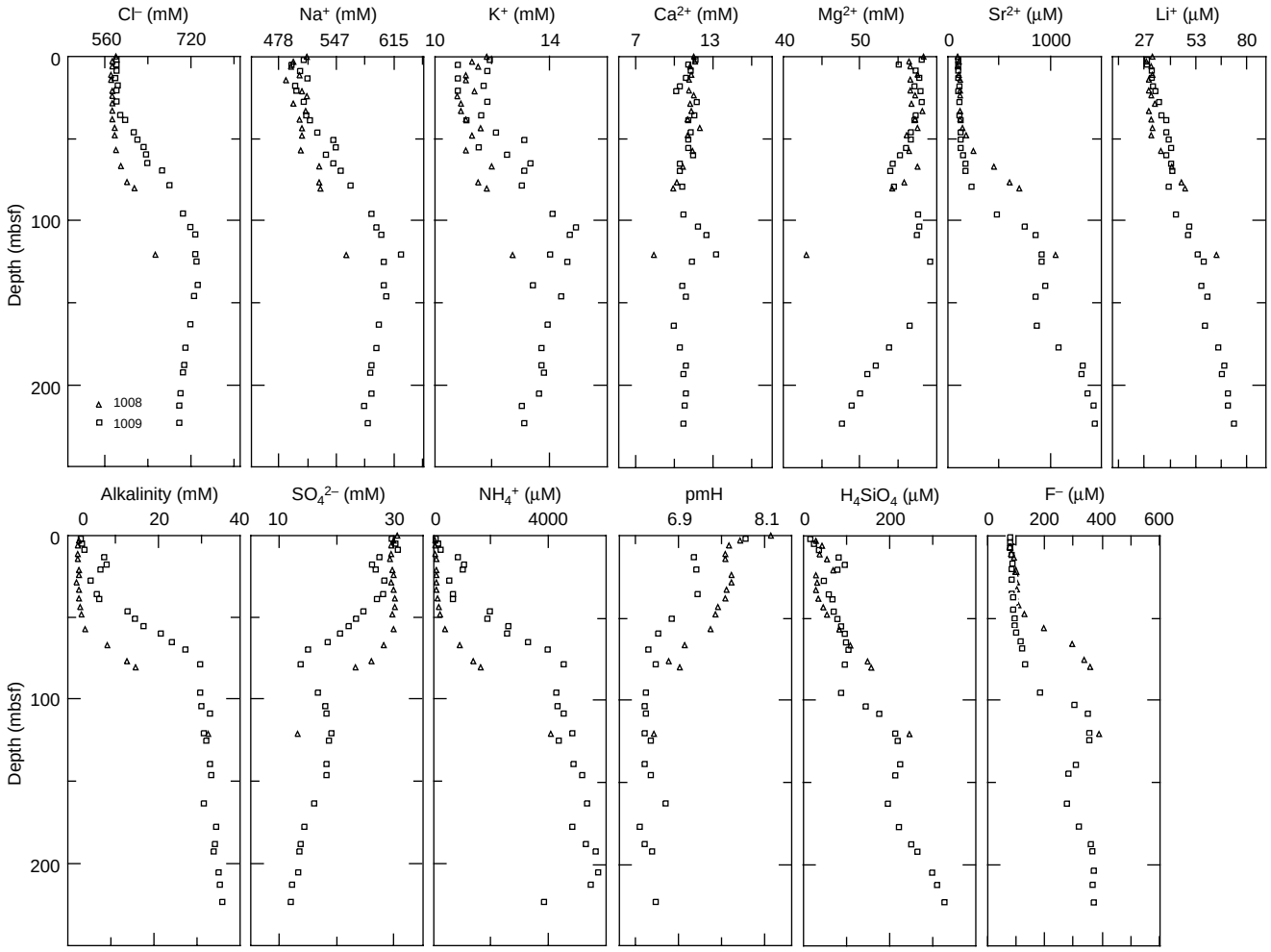

Figure 23. Depth profiles of interstitial water constituents at Sites 1008 and 1009.

are given in Table 7. Figures 23 and 24 show concentration profiles and the ratios of selected constituents, respectively.

The mineralogy of the carbonate portion of the sediments at Site 1004 was quantified by X-ray diffraction (XRD) at a frequency of one sample every other section (Table 8 on CD-ROM; Fig. 25). A total of 105 samples were analyzed. All carbonate mineralogy data were corrected to include the noncarbonate fraction as determined by total carbonate analysis (see "Organic Chemistry" section, this chapter).

Interstitial Waters

Site 1008

Salinity, Chloride, Sodium, and Potassium

Salinity, chloride (Cl^-), and sodium (Na^+) profiles at Site 1008 show little change in the upper portion of the sediments (0–50 mbsf). Below this zone, each of these constituents increases gradually to the bottom of the hole, where maximum values of 40, 653 mM, and 559 mM were observed, respectively. Although there appears to be a slight decrease in the concentration of potassium (K^+) between 20 and 40 mbsf (Fig. 23), there is significant scatter in the data for this constituent by ion chromatography (see "Explanatory Notes" chapter, this volume), and this trend may be artificial. Dissolved K^+ reaches a maximum of 12.7 mM at 120 mbsf and decreases slightly farther downhole. Within the accuracy of the technique, both Na^+ and K^+ concentrations behave conservatively with respect to seawater ratios.

Calcium, Magnesium, Strontium, and Lithium

Dissolved calcium (Ca^{2+}) and magnesium (Mg^{2+}) remain in a narrow range of concentration to approximately 50 mbsf, below which both constituents display a slight decrease to 8.0 mM and 43.0 mM, respectively, at 120 mbsf. The concentration of dissolved strontium (Sr^{2+}), however, increases below 40 mbsf, rising smoothly from a range of 100–124 µM to a maximum of 1057 µM at 120 mbsf. Dissolved lithium (Li^+) remains relatively constant in the first 40 mbsf, subsequently rising to a maximum of 64 µM at 120 mbsf.

Alkalinity, Sulfate, Ammonium, Phosphate, and pmH

The titration alkalinity, sulfate (SO_4^{2-}), and ammonium (NH_4^+) concentrations at Site 1008 show significant changes below approximately 40 mbsf, although both SO_4^{2-} and NH_4^+ exhibit some variations between 11 and 20 mbsf (Table 7). The alkalinity increases to a maximum of 32.8 mM at 120 mbsf and is nearly balanced stoichiometrically (2:1 ratio) by a depletion of SO_4^{2-} over this depth range. Dissolved NH_4^+ increases from approximately 100 µM to near 4000 µM between 40 and 120 mbsf.

The dissolved phosphate (HPO_4^{2-}) concentrations range between 1 and 5.7 µM, showing a highly variable distribution throughout the core (not shown). The pmH of the interstitial water at Site 1008 exhibits a decrease immediately below the mudline from 7.71 to 7.52 that coincides with the small increase in NH_4^+ near 20 mbsf. Below this depth, pmH increases slightly to 7.63 before decreasing again below 24 mbsf to a minimum of 6.56 at 120 mbsf.

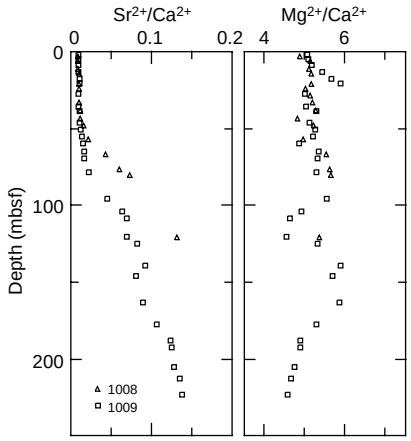

Figure 24. Depth profiles of Sr^{2+}/Ca^{2+} and Mg^{2+}/Ca^{2+} in interstitial water parameter ratios.

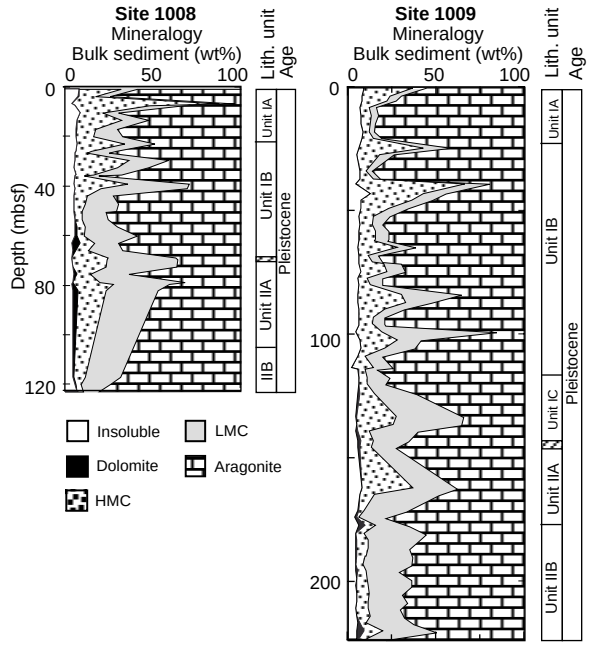

Figure 25. Quantitative X-ray mineralogy of sediments from Sites 1008/1009.

Silica, Fluoride, and Iron

The silica (H_4SiO_4) profile at Site 1008 shows two reaction zones. The first occurs in the upper 25 mbsf and is characterized by an increase from 29 µM at 3 mbsf to 71 µM at 26 mbsf. Below this depth H_4SiO_4 returns to approximately 30 µM before rising gradually to 246 µM at 120 mbsf.

Dissolved fluoride (F^-) displays a small increase from seawater concentrations (~70 µm) over the upper 20 mbsf (85–100 µm), followed by a relatively constant concentration to 43 mbsf. Below this depth F^- increases to 310 µM at 120 mbsf. The shape of the profile (Fig. 23) suggests the existence of a broad maximum in the F^- concentration near 100–120 mbsf.

Iron (Fe^{2+}) concentrations at Site 1008 remain low (3.3–6.9 µM) within the upper 66 mbsf. A single-point maximum of 14 µM at 69 mbsf probably is associated with release from the sediments as they become more reducing. Below this depth, Fe^{2+} decreases to less than 3-µM Fe^{3+}, possibly reflecting removal as an insoluble sulfide.

Site 1009

Salinity, Chloride, Sodium, and Potassium

The salinity and Cl^- display no significant variability in the upper 30 mbsf at Site 1009; these parameters subsequently increase to maxima of 46 and 725–730 mM, respectively between 110 and 140 mbsf before decreasing farther downhole. The dissolved Na^+ profile generally follows that of Cl^-. Dissolved K^+ exhibits much greater scatter than that observed at prior sites on this leg, although the general trend also appears to follow those of the other conservative constituents.

Calcium, Magnesium, Strontium, and Lithium

Although, the Ca^{2+} profile at Site 1009 shows concentrations close to seawater values throughout, there are small deviations at 35 and 120 mbsf (Fig. 23; Table 7). Except for a small decrease at 64 mbsf, concentrations of Mg^{2+} are elevated above seawater values (58–61 mM). Below 145 mbsf, Mg^{2+} decreases reaching a minimum of 47.6 mM at 223 mbsf.

As observed at Sites 1006 and 1007, Sr^{2+} exhibits a small but significant increase over seawater concentrations (94 µM) immediately below the seafloor. Concentrations remain in a narrow range of 97–110 µM down to 35 mbsf, below which a gradual increase occurs to 75 mbsf. Below this depth, dissolved Sr^{2+} increases sharply, displaying a submaximum of 948 µM at 142 mbsf. After a slight decrease, Sr^{2+} concentrations increase further to 1433 µM at 217 mbsf.

Unlike Sr^{2+}, the concentration of Li^+ begins to increase immediately below the seafloor. A nearly linear increase from 28 to 40 µM occurs down to 54 mbsf, followed by a less regular trend over the next 40 m, and a more regular increase to 73 µM at 217 mbsf.

Alkalinity, Sulfate, Ammonium, Phosphate, and pmH

Alkalinity, SO_4^{2-}, and NH_4^+ covary within three generalized zones at Site 1009. The first of these zones extends from the seafloor to 40 mbsf, and contains a small maxima in alkalinity (9 mM) and NH_4^+ (1047 µM), and a minimum in SO_4^{2-} (26 mM) at 17 mbsf (Fig. 23). A second zone (40–78 mbsf) is characterized by sharp increases in alkalinity (30.8 mM) and NH_4^+ (4500 µM), and a corresponding minimum in SO_4^{2-} (13.7 mM). This zone is interpreted to be a sulfate reduction zone. A third zone extends from 78 mbsf to the base of the hole and is marked by a flattening of all three profiles.

Dissolved HPO_4^{2-} concentrations are relatively low and highly variable throughout Site 1009. A range of 1 to 7 µM is observed, with higher concentrations generally occurring within the sulfate-reduction zone.

The pmH profile at Site 1009 is consistent with the observed variations in the interstitial water parameters associated with the remineralization of organic matter. A decrease from 7.78 to 7.10 occurs immediately below the mudline, coinciding with the local maxima in NH_4^+ and alkalinity near 20 mbsf. The pmH remains nearly constant down to 35 mbsf before decreasing further in the sulfate-reduction zone. Below approximately 70 mbsf, the pmH remains in a range of 6.4–6.7.

Silica, Fluoride, and Iron

The H_4SiO_4 profile at Site 1009 is somewhat similar to that observed at Site 1008, although several other reaction zones may be identified. A first small, local H_4SiO_4 maximum (94 µM) at 17 mbsf occurs approximately 3 m shallower than at Site 1008. Between 120 and 140 mbsf, another maximum of 103 µM is observed. Between 100 and 125 mbsf the increase in H_4SiO_4 225 µM corresponds closely to the maximum value of 246 µM observed at 120 mbsf at Site 1008. A more pronounced increase in H_4SiO_4 occurs downhole, with a concentration of 327 µM at the bottom of Site 1009.

Dissolved F^- increases gradually (77–113 µM) in the first 64 mbsf of Site 1009 before exhibiting a more pronounced increase down to 75 mbsf. Below this depth, fluoride continues to increase, reaching a concentration of 373 µm at the bottom of the hole.

Fe^{2+} concentrations at Site 1009 are more variable than at Site 1008, exhibiting a range of 2–17 µM. Local dissolved Fe^{3+} maxima correspond to those in alkalinity and minima in SO_4^{2-}, although they are generally poorly defined.

Summary of Interstitial Water Results

As observed at the northern sites of the Bahamas Transect, the upper portion of Sites 1008 and 1009 appears to display evidence of fluid flow. The flushed zone observed at Sites 1008 and 1009, however, is shallower and less well defined than at Sites 1003–1005 and does not appear as well constrained by lithologic boundaries. Evidence for deeper fluid flow may exist in the form of the local decrease in salinity and other conservative constituents observed below 125 mbsf at Site 1009.

The profiles of interstitial water constituents at Sites 1008 and 1009 reflect the microbial degradation of organic matter, recrystallization of biogenic carbonates, and silica diagenesis. Several localized reaction zones also appear to influence the shape of the profiles at Site 1009, although these are less well defined at Site 1008.

Evidence of carbonate remineralization at Sites 1008/1009 is derived primarily from variations in the Sr^{2+}/Ca^{2+} and Mg^{2+}/Ca^{2+} ratios (Fig. 24) and increases in the Sr^{2+} concentrations immediately below the seafloor. In the upper 40–50 mbsf, slight increases in both Ca^{2+} and Sr^{2+}, accompanied by only a very small change in the Sr^{2+}/Ca^{2+} ratio, suggest that aragonite may be undergoing dissolution (Baker et al., 1982). Below 50 mbsf, however, the significant increase in the Sr^{2+}/Ca^{2+} indicates the active recrystallization of aragonite. An increase in the Mg^{2+}/Ca^{2+} observed in the first 20 mbsf at Site 1009 may also reflect the dissolution of high-magnesium calcite (HMC). It is possible that dolomitization reactions are important below 150 mbsf at Site 1009, causing the Sr^{2+}/Ca^{2+} to increase and the Mg^{2+}/Ca^{2+} to decrease. Dissolved Sr^{2+} concentrations appear to be controlled by the solubility of celestite ($SrSO_4$) below approximately 120 mbsf.

The alkalinity increases within the zone of active microbial degradation at both sites are of the same order of magnitude as observed at Sites 1003–1005 and are nearly stoichiometrically balanced by a loss of SO_4^{2-} (Fig. 23). The release of NH_4^+ that accompanies this alkalinity increase is also approximately that expected from degradation of marine organic matter. The amount of HPO_4^{2-} observed in the sediments is less than expected. The deficiency in this highly surface active constituent may be attributed to adsorption onto other phases such as carbonates or detrital oxides (Kitano et al., 1978; Gaudett and Lyons, 1980).

Mineralogy

The mineralogy of Sites 1008/1009 is dominated by a mixture of aragonite, high-magnesium calcite (HMC), and low-magnesium calcite (LMC), and dolomite. Dolomite is the least abundant of these phases and appears only below approximately 50 mbsf at Site 1008 and below 110 mbsf at Site 1009. Carbonates form approximately 95 wt% or more of the bulk sediments; the remainder most likely consists of organic carbon, biogenic silica, and clays (see "Organic Geochemistry" section, this chapter).

The most striking feature in both cores is the cyclicity in the abundances of aragonite and HMC. These variations occur in distinct cycles, which probably correspond to high-frequency glacial sea-level changes throughout the Pleistocene (see "Lithostratigraphy" section, this chapter). The cyclicity is observed primarily above 80 mbsf at Site 1008, whereas at Site 1009, which is characterized by greater sedimentation rates (see "Biostratigraphy" section, this chapter), the cyclicity extends to depths greater than 150 mbsf. Within these cycles, the abundance of HMC and LMC increases noticeably at the aragonite minima, probably reflecting the increased role of marine seafloor cementation during sea-level lowstands (Schlager and James, 1978).

PHYSICAL PROPERTIES

Measurements of physical properties at Sites 1008/1009 were conducted following the procedures described in the "Physical Properties" section of the "Explanatory Notes" chapter (this volume). Two to six discrete measurements of *P*-wave velocity and one or two measurements of shear strength were taken in every section of unconsolidated cores. Index property samples were measured every other section. In semilithified cores, approximately five velocity measurements were taken per section. Thermal conductivity was measured on unconsolidated whole cores with a frequency of one per section to 120 mbsf at Site 1008 and to 180 mbsf at Site 1009.

The following describes the downhole variation in petrophysical properties and their correlation with lithostratigraphy for each site. Variations in magnetic susceptibility are described within the "Paleomagnetism" section (this chapter).

Site 1008 Index Properties, GRAPE Density, and *P*-Wave Velocity

Tables 9 through 14 on CD-ROM summarize the measurements of index properties, discrete DSV velocity, GRAPE density, PWL velocity, magnetic susceptibility, and NGR at Site 1008.

At Site 1008, the petrophysical properties show regular, repetitive downcore variations at scales ranging from approximately 5 to 20 m in thickness (Fig. 26). Downcore, *P*-wave velocities range from 1.55 to 1.75 km/s with peaks up to 4.3 km/s. Bulk density varies between 1.7 and 2.15 g/cm^3. GRAPE density is slightly higher, but follows a similar trend (see "Explanatory Notes" chapter, this volume). Porosity ranges from 21% to 65%. Except for the first 5 mbsf, which is characterized by very low gamma emission, natural gamma ray has values between 10 and 25 cps with a gradual increase in the baseline downcore.

On the basis of *P*-wave velocity and bulk density, two petrophysical units were defined. Petrophysical Unit I (0 to 39 mbsf) has bulk densities between 1.75 and 2.4 g/cm^3 with a gradual baseline increase downcore. *P*-wave velocity, bulk density, and gamma ray within Unit I show five well-defined cycles. These cycles have relatively low values of velocity, density, and gamma ray at the base that increase upcore to high values near the top (Fig. 26). Many of these petrophysical cycles coincide with the coarsening-upward depositional intervals, which are characterized by unconsolidated ooze to wackestone that coarsens upward to unlithified lithoclastic floatstones (see "Lithostratigraphy" section, this chapter). However, these cycles in the petrophysical profiles are more numerous than the cycles in the cores. Within petrophysical Subunit Ia, natural gamma ray is flat and has values well below the background radiation level of 6 cps. This subunit is probably the Holocene sequence. The transition from lithologic Subunit IA to Subunit IB coincides with a cycle boundary within petrophysical Subunit Ib.

Petrophysical Unit II (39–122 mbsf) has bulk densities between 1.95 and 2.15 g/cm^3. The upper portion of this interval, Subunit IIa (39–79 mbsf) has at least five petrophysical cycles that are based on variations in bulk density, velocity, and gamma ray, whereas only two were recorded in the cores. Petrophysical Subunit IIb (79–122 mbsf) is in an interval of low recovery, and therefore little information is available on the downcore variation in petrophysical properties. Overall, the range in petrophysical properties is close to that in Subunit IIa.

Site 1008 Shear Strength

Shear strength was measured on unconsolidated sediments down to a depth of 120 mbsf (Table 15 on CD-ROM; Fig. 27). The measurements show a gradual downcore increase to values ranging from 10 to 25 kPa at a depth of approximately 60 mbsf. Except for the first

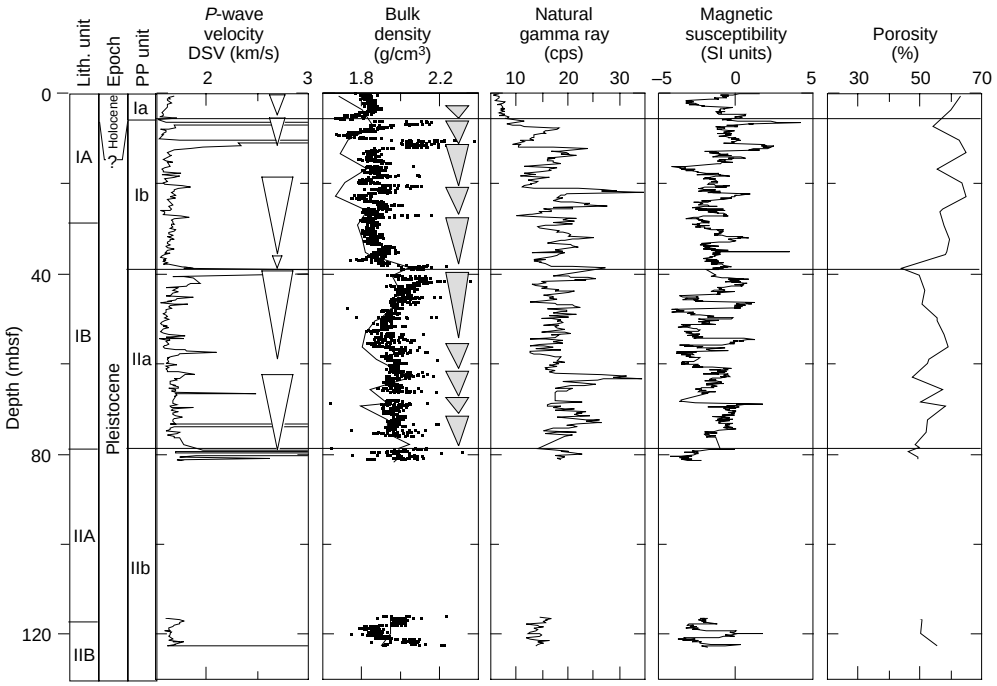

Figure 26. Combined plot of *P*-wave velocity from the DSV, porosity and bulk density from discrete measurements, NGR, magnetic susceptibility from the MST, and porosity from Site 1008. Lithologic and petrophysical units are indicated along with age. Depositional cycles (see also "Lithostratigraphy" section, this chapter) and petrophysical cycles are indicated by open and shaded triangles, respectively.

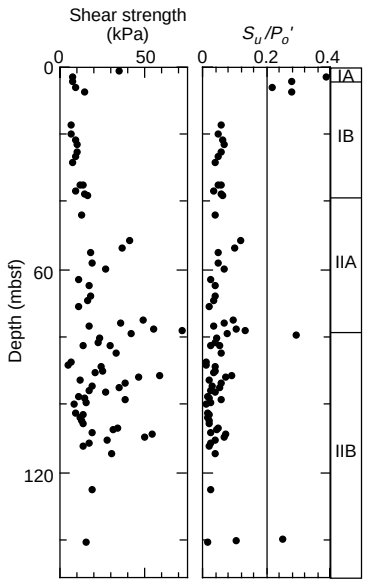

Figure 27. Shear strength and S_u/P_o' calculated from shear strength and overburden stress for cores from Site 1008.

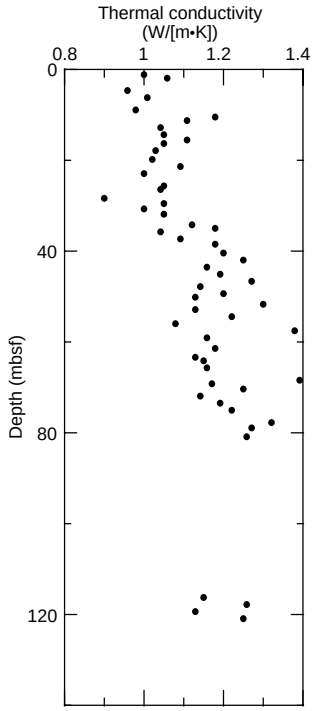

Figure 28. Thermal conductivity at Site 1008.

10 mbsf, the S_u/P_o' ratios are well below 0.2. At 60 mbsf, shear strength increases up to values of 50 kPa and higher. This rather abrupt downcore increase in shear strength coincides with the top of one of the depositional successions described earlier (between 62 and 78 mbsf; see Fig. 26).

Site 1008 Thermal Conductivity

A total of 57 thermal conductivity measurements were made to a depth of 120 mbsf at Hole 1008A (Table 16 on CD-ROM; Fig. 28). Thermal conductivity at this site is highly variable downcore. It increases from near 1.0 to 1.1 W/(m·K) in the upper 15 mbsf and then decreases downcore to 1.05 W/(m·K) at about 35 mbsf. Below this depth, thermal conductivity increases sharply to 1.2 W/(m·K) at 40 mbsf. A similar increase is observed also in the bulk density and *P*-wave velocity. Thermal conductivity is then variable downcore, averaging 1.2 W/(m·K). Measurements from 90 through 115 mbsf are

limited because of poor core recovery. The average of all measurements is 1.14 W/(m·K) and the standard deviation is 0.1 W/(m·K).

Site 1009 Index Properties, GRAPE Density, and *P*-Wave Velocity

Tables 17 through 22 on CD-ROM summarize the measurements of index properties, discrete DSV velocity, GRAPE density, PWL velocity, magnetic susceptibility, and NGR from Site 1009.

Petrophysical properties at Site 1009 display similar repetitive downcore variations as seen at Site 1008. The thickness of these cycles, marked by velocity, density, and gamma-ray variations, ranges from approximately 5 up to 20 m and averages 10 m (Fig. 29). Overall, velocity ranges from 1.5 to 1.75 km/s with peaks up to 4.3 km/s. Bulk density has values between 1.65 and 2.0 g/cm^3 and shows a subtle downcore increase in the baseline value. Natural gamma ray has values between 10 and 20 cps but no apparent downcore trend. Variations in *P*-wave velocity, bulk density, and gamma ray allow subdivision into three petrophysical units.

Petrophysical Unit I (0–21 mbsf) has velocities between 1.5 and 1.6 km/s, bulk densities between 1.75 and 1.85 g/cm^3, and gamma-ray emissions close to the background level. The transition to the underlying unit at 21 mbsf is represented by a sharp increase in velocity, bulk density, and gamma ray. It corresponds to a downcore shift to more consolidated foraminifer ooze and wackestone and the presence of lithified packstone to grainstone layers and hardgrounds. Petrophysical Unit I probably represents the Holocene section.

Petrophysical Unit II (21–161 mbsf) contains at least 15 cycles of downcore-decreasing velocity, density, and gamma ray. Most, but not all, of these petrophysical cycles correspond to recorded depositional successions similar to those observed at Site 1008 (see "Lithostratigraphy" section, this chapter). Bulk density displays the most complete record of these cycles. The lower boundary of Unit II is located at the top of a low-recovery interval (~150–160 mbsf) and indicates a sharp downcore shift to lower bulk densities, down to 1.7 g/cm^3. Within petrophysical Unit II, porosity shows a baseline shift from approximately 60% to 50%. No distinct downcore trend in velocity or gamma ray is observed. However, magnetic susceptibility shows a significant shift to higher, positive values at this depth.

Petrophysical Unit III (161–224 mbsf) has no distinct petrophysical cycles, but shows a gradual upcore decrease in bulk density values toward the top of the unit. The unit is characterized by relatively invariant velocities ranging from 1.55 to 1.6 km/s, densities between 1.9 and 2.0 g/cm^3, and gamma-ray values between 10 and 15 cps.

Only the change from petrophysical Unit I to Unit II coincides with a boundary between lithologic units. Other lithologic unit boundaries fall near the tops of petrophysical cycles.

Site 1009 Shear Strength

At Site 1009, shear strength was measured on unconsolidated sediments down to a depth of 140 mbsf (Table 23 on CD-ROM; Fig. 30). Shear strength increases downcore, in the upper 50 mbsf, from values between 5 and 15 kPa to values that range between 5 and 75 kPa at a depth of 140 mbsf. S_u/P_o' ratios are usually lower than 0.1 and display a sawtooth pattern of intervals with downcore-decreasing ratios that, surprisingly, cannot be correlated directly with petrophysical cycles (see also Fig. 30).

Site 1009 Thermal Conductivity

A total of 86 thermal conductivity measurements were made from 0 to 181 mbsf of Hole 1009A (Table 24 on CD-ROM; Fig. 31). In the upper 140 mbsf, thermal conductivity remains relatively constant, with an average of about 1.1 W/(m·K). The number of measurements made from 140 through 160 mbsf is limited because of poor core recovery. From 160 to 180 mbsf, thermal conductivity increases sharply downcore from near 1.0 to 1.2 W/(m·K). The average of all measurements is 1.09 W/(m·K) and the standard deviation is 0.07 W/(m·K).

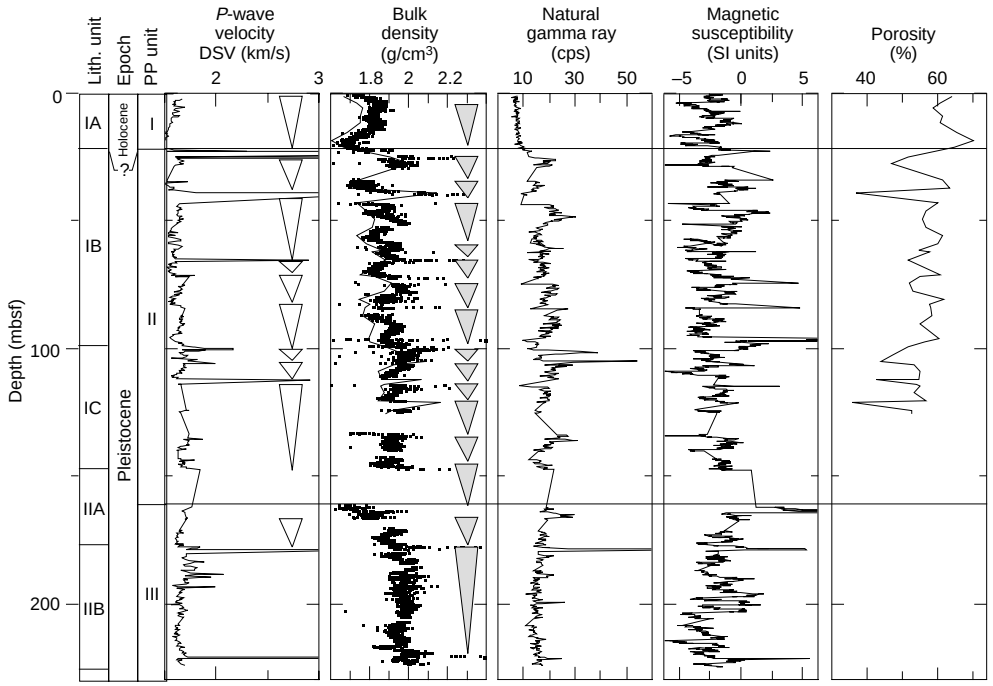

Figure 29. Combined plot of the *P*-wave velocity from the DSV, bulk density from discrete measurements (line) and GRAPE density (points), NGR, magnetic susceptibility, and porosity from Site 1009. Petrophysical and lithologic units are indicated along with age. Depositional cycles (see also "Lithostratigraphy" section, this chapter) and petrophysical cycles are indicated by open and shaded triangles, respectively.

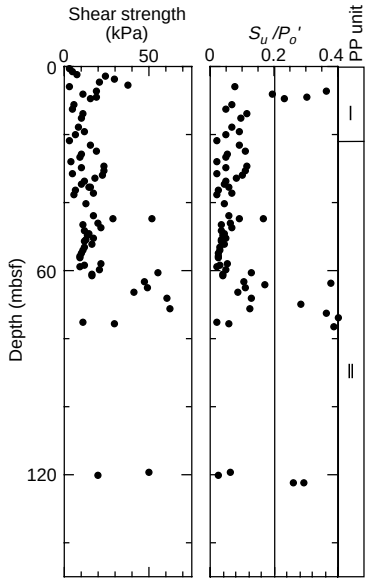

Figure 30. Shear strength and S_u/P_o' calculated from shear strength and overburden stress for cores from Site 1009.

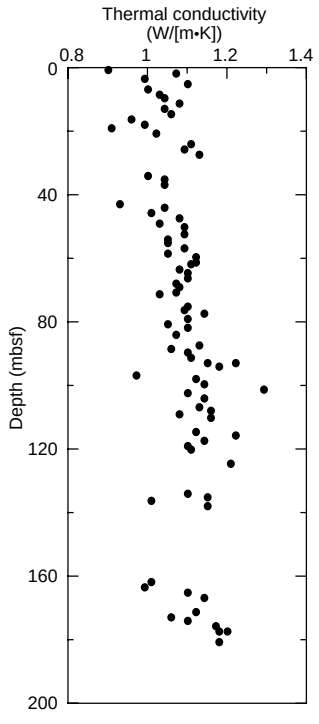

Figure 31. Thermal conductivity for Site 1009.

IN SITU TEMPERATURE MEASUREMENTS

Introduction

At Site 1008, seven in situ temperature measurements were made using two sets of Adara tools and one unit of downhole water sampler, temperature, and pressure probes (WSTP). The measurements and errors (Table 25) are described in the "In Situ Temperature Measurements" section of the "Explanatory Notes" and "Site 1003" chapters, this volume. The temperature at the seafloor (17.1°C) has been obtained from the mudline stops.

Table 25. In situ bottom-hole sediment temperatures measured at Site 1008.

Core	Depth (mbsf)	Temperature (°C)	Error (°C)	Mudline (°C)	Tool
166-1008A-					
3H	25.6	16.94	0.15	17.03	Adara11
4H	35.1	16.88	0.12	17.20	Adara18
5H	40.2	17.01	0.25	16.98	Adara11
6H	49.7	17.32	0.10	17.10	Adara18
7H	59.2	17.23	0.15	17.06	Adara11
8H	68.7	17.46	0.15	17.12	Adara18
14X	106.8	18.50	0.20		WSTP201

At Site 1009, 10 in situ temperature measurements were made using two sets of Adara tools and one unit of WSTP (Table 26). The temperature at the seafloor (18.2°C) has been obtained from the mudline stops.

Geothermal Profile: Site 1008

The geothermal profile at Site 1008 is shown in Figure 32. The temperatures are nearly constant in the upper 60 mbsf, although they increase slightly with depth. All of the Adara measurements are considered to be fairly reliable. The penetration temperature record from Core 166-1008A-4H is shown in Figure 33 as an example. The three measurements below 60 mbsf fall on a straight line with a gradient of 26.9°C/km.

The geothermal profile shows a concave upward feature that has been commonly observed at the northern Leg 166 sites. Either historical fluctuation of the bottom-water temperature or an influx of seawater into the shallow zone of the sediments could explain the occurrence of this feature. Another important characteristic of the profile is that the geothermal gradient is lower than at any of the previous sites by at least 20%. The profile from Site 1004, which is located on nearly the same water depth in the northern drilling transect, is shown in Figure 32 for comparison. At Site 1008, there exists a shallow zone of sediments in the upper 50 mbsf with no salinity gradient, which is interpreted as a "flushed zone" where normal seawater advectively penetrates (see "Inorganic Geochemistry" section, this chapter). The thickness of this zone is comparable to that of the zone of near-zero geothermal gradient. The low geothermal gradient and the concave profile may therefore be caused by influx of seawater.

Geothermal Profile: Site 1009

Site 1009 shows a linear geothermal profile (Fig. 34). Some shallow measurements deviate from this trend, but they are less reliable than the others as the advanced hydraulic piston corer (APC) did not fully penetrate (Cores 166-1009A-5H and 6H). The geothermal gradient based on the five measurements below 70 mbsf is 16.8°C/km.

Heat Flow: Site 1008

The heat flow value at this site (30.5 mW/m^2) has been calculated from the geothermal gradient of the three measurements below 59 mbsf (26.8°C/km) and the average of the thermal conductivities in the same depth range (1.14 W/[m·K]). The heat flow value is significantly lower than that of the previous sites, reflecting the low geothermal gradient. If the regional heat flow of this area is nearly the same as that of the northern sites (39 mW/m^2 at Site 1004), then effects such as fluid migration must suppress the heat flow by about 30%.

Heat Flow: Site 1009

The heat flow value at Site 1009 (18.8 mW/m^2) has been calculated from the geothermal gradient of the five measurements below 70 mbsf (16.8°C/km) and the average of the thermal conductivities in

Table 26. In situ bottom-hole sediment temperatures measured at Site 1009.

Core	Depth (mbsf)	Temperature (°C)	Error (°C)	Mudline (°C)	Tool	Notes
166-1009A-						
3H	23.8	18.93	0.23	18.32	Adara11	
4H	33.3	18.80	0.1	18.59	Adara18	APC partial stroke
5H	38.3	18.35	0.3	18.94	Adara11	APC partial stroke
6H	42.3	19.34	0.5	18.44	Adara18	APC partial stroke
7H	51.8	19.09	0.1	19.30	Adara11	
11H	73.8	19.38	0.1	19.20	WSTP201	
14H	95.8	19.76	0.2	18.95	WSTP201	
18X	123.5	20.16	0.1	18.16	WSTP201	
21X	152.0	20.66	0.1	18.31	WSTP201	
24X	180.1	21.18	0.1	18.45	WSTP201	

Note: APC = advanced hydraulic piston corer.

the same depth range (1.12 W/[m·K]). This heat flow value is the lowest of all the Leg 166 sites. It is also lower than that of neighboring Site 1008 by 38%. The large variation in heat flow within the relatively short distance (3.6 km) suggests an anomaly in the local geothermal regime at Site 1009. Part of the difference between the two sites may be explained by the rapid sedimentation rate at Site 1009. The rate was as high as about 380 m/m.y. from 0.5 Ma to 0.25 Ma. This could suppress the heat flow through the seafloor by 10% or more. It may also be suspected that this site is located at or near a major hydrological recharge zone. However, there is no evidence of such a zone based on the geochemical profiles, and deeper drilling may be necessary to ascertain whether such a zone is present.

SEISMIC STRATIGRAPHY

Introduction

Sites 1008/1009 are located 100 km south of the main Bahamas Transect at locations that are, respectively, 2.5 and 6 km seaward of the modern platform margin. Compared with the steep margin along the northern transect (Sites 1003–1007), the margin at the southern sites has a more gently dipping profile (Fig. 4). The two holes were drilled to a depth of 134.5 and 226.1 m respectively, and provide, together with seismic Line FS4, insight into the sequence stratigraphic architecture of the youngest Pleistocene–Holocene history of the progradation of the Great Bahama Bank (Fig. 35). Seismic section FS4 was acquired with the same multichannel system used for the main Bahamas Transect (see "Site Survey and Underway Geophysics" chapter, this volume). However, since the main focus at these sites is to image the uppermost 200 m, we did not stack this section because stacking results in smearing of the reflections, in particular for shallow-dipping layers. To preserve the highest possible resolution, only one channel of the acquired seismic data was processed (filtered and gained), which proved to be the best method to image the youngest seismic sequences at those shallow depths (Fig. 35). Eight seismic sequences were recognized and named *s*–*y*. Their basal seismic sequence boundaries (SSB S–Y) are defined on the basis of reflection terminations and stratal geometry. Their characteristics and correlation to the cores are discussed in the following paragraphs.

Time-Depth Conversion

To select a time-depth conversion for Sites 1008/1009, we compared the shallow portions of the check-shot surveys of the northern Leg 166 sites (Fig. 36). Because the lithologies at Sites 1008/1009 are relatively unconsolidated, the slowest available VSP curve from Site 1006 was selected, because it had the shallowest check-shot station of all surveys (106 mbsf). The upper 200 m at Site 1006 also shows similar acoustic properties to Sites 1008/1009. The time-depth curve from Site 1006 was simplified with a best-fit linear time-depth curve

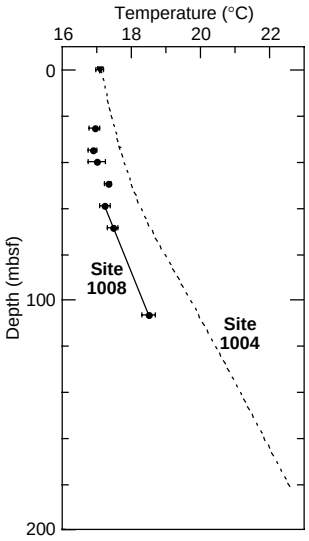

Figure 32. Geothermal profile at Site 1008.

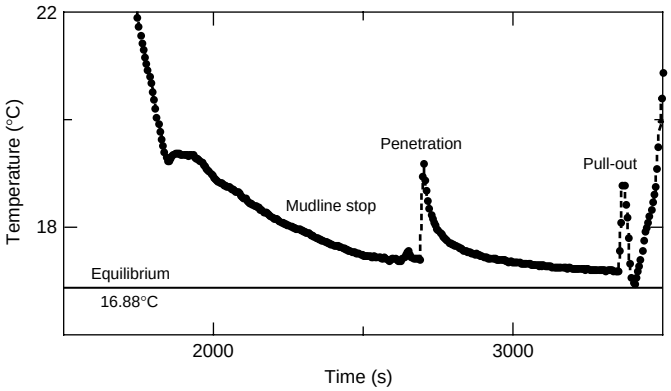

Figure 33. Adara penetration temperature record from Core 166-1008A-4H.

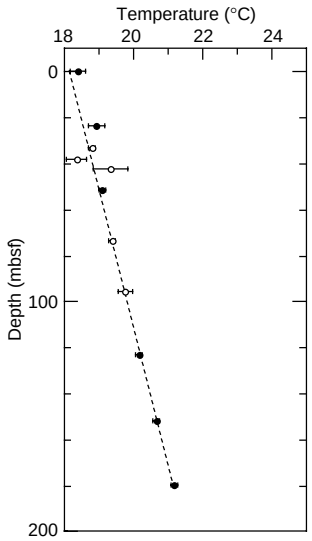

Figure 34. Geothermal profile at Site 1009. Solid circles = the reliable temperature measurements, and open circles = unreliable ones.

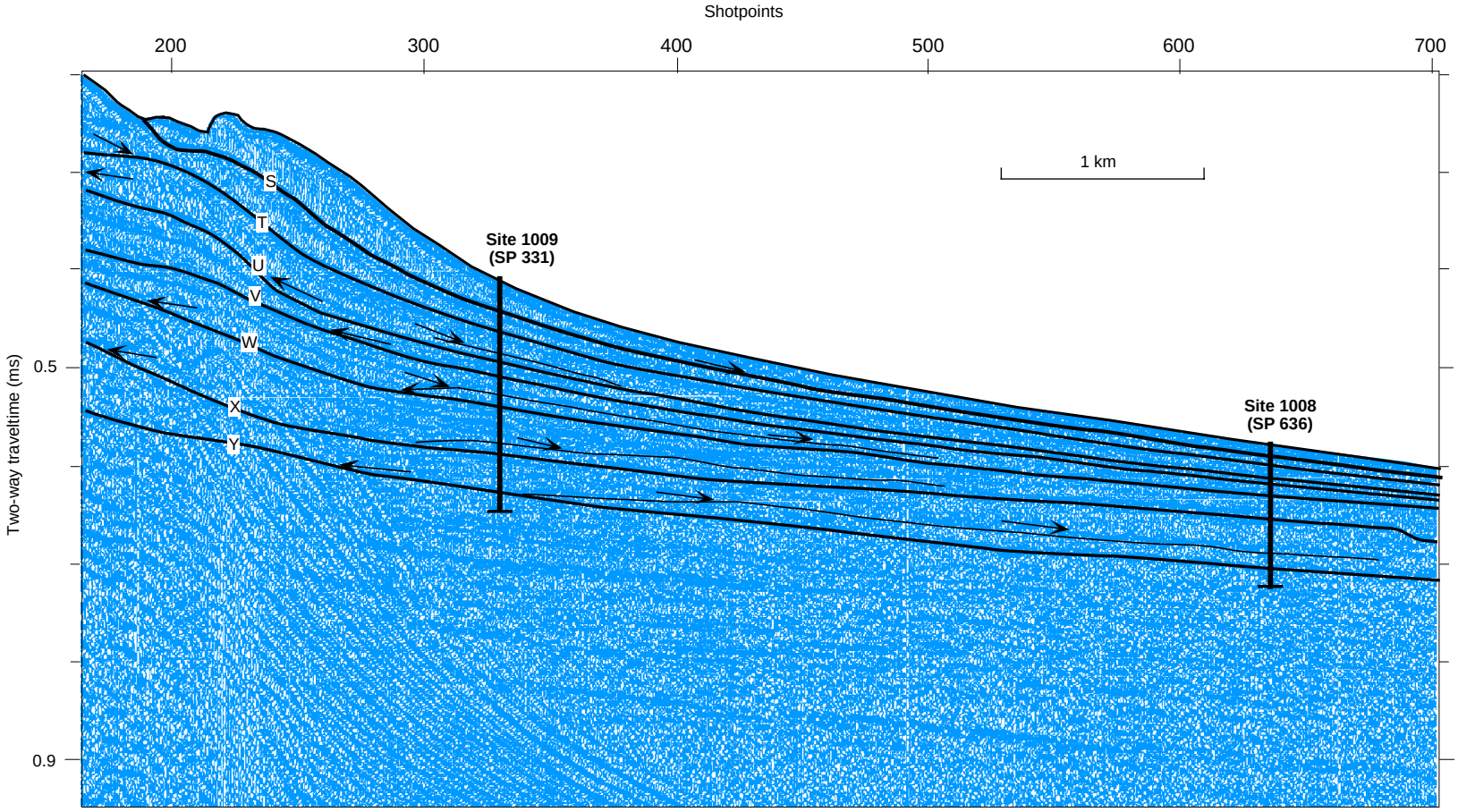

Figure 35. A portion of seismic Line FS4 showing locations of Sites 1008 and 1009. Based on onlap patterns, eight seismic sequences could be distinguished. Within the sequences, reflections show frequent downlapping terminations onto sequence-internal reflections, which indicate slope-confined units deposited during sea-level lowstands.

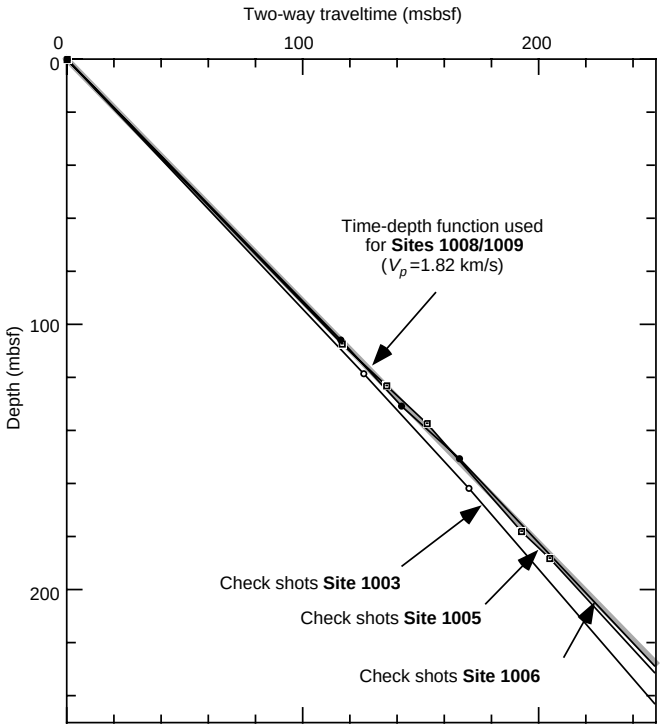

Figure 36. Time-depth correlation used for Sites 1008/1009 compared with VSP check-shot surveys of Sites 1003, 1005, and 1006. The small differences between check-shot curves above 200 mbsf, and the similarity of acoustic properties between Sites 1006 and 1008/1009 justify the use of a simplified linear curve, which was derived from a best-fit through the Site 1006 check shots.

representing a velocity of 1.82 km/s. The resulting conversion line is plotted in Figure 36.

Pleistocene-Holocene Sequences

Eight seismic sequences (*s*–*z*) can be recognized in the drilled section. These are separated from each other by seven SSBs (SSB S–Y, Table 27). The SSBs are recognized in the proximal zone below the modern platform margin by onlap surfaces (Fig. 35). The sequences are characterized in the more distal areas by distinct downlapping reflections, which usually terminate on a sequence-internal reflection, indicating a depositional package that is confined to the slope (lowstand wedge).

Most of the SSBs correlate with distinct layers in the cores that are dark in color, coarse-grained, and show signs of intense submarine cementation (Fig. 37; also see "Lithostratigraphy" section, this chapter). These cemented layers are characterized by sharp velocity, density and gamma-ray spikes, and mark the top of coarsening-upward cycles clearly seen in both petrophysical and lithologic changes (Figs. 37, 26, 27). These coarsening-upward cycles are sometimes capped by very fine-grained, clay-rich layers. These petrophysical signatures contrast clearly with the more homogenous, low-velocity and low-density signature of the light-colored background sediments.

The youngest seismic sequence, *s*, appears at Site 1009 at 29 mbsf and at Site 1008 at 9.6 mbsf. The estimated age is 0.15 and 0.12 Ma, respectively, at Sites 1009 and 1008, which makes this boundary likely to be the result of the last sea-level lowstand (Table 27) (see "Biostratigraphy" section, this chapter). This assumption is supported by the fact that this surface coincides with the first downhole appearance of a coarse and cemented layer at 21 mbsf at Site 1009 and at 5 mbsf at Site 1008.

Table 27. Compilation of time-depth conversion and tentative age assignments of seismic sequence boundaries at Sites 1008/1009.

	Site 1009			Site 1008		
Seismic sequence boundary	TWT below seafloor (msbsf)	Depth (mbsf)	Age* (Ma)	TWT below seafloor (msbsf)	Depth (mbsf)	Age* (Ma)
S	31.9	29	0.15	10.6	9.6	0.12
T	53.2	48.4	0.25	16	14.5	0.2
U	79.8	72.6	0.32	26.6	24.2	0.25
V	106	96.8	0.4	42.6	38.7	0.4
W	138	126	0.7	58.5	53.2	0.62
X	191	174	1.2	85.1	77.4	0.91
Y	229	208	1.3–1.4	138	126	?

Note: * = ages are preliminary and based on shipboard biostratigraphy (see "Biostratigraphy" section, "Explanatory Notes" chapter, this volume).

SSB T occurs at 48 mbsf at Site 1009 and 14.5 mbsf at Site 1008 and matches well with the second dark-colored layer observed in the cores at 40 and 10 mbsf, respectively. The estimated ages for this SSB are 0.2 and 0.25 Ma. SSB U (73 mbsf at 1009 and 24 mbsf at 1008) has, at Site 1009, a petrophysical signature in the cores with a high-velocity layer at 66 mbsf, while only a smaller-scale velocity excursion is recognized at Site 1008. SSBs S, T, and U occur at slightly deeper depths than the high-velocity layers observed at both sites (Fig. 37). This small offset may be the result of actual velocities being slightly lower than those assumed for the upper portion of the section. SSB V (97 mbsf at 1009 and 39 mbsf at 1008) correlates in both sites with the top of one of the best expressed lithologic cycles at 100 mbsf (Site 1009) and 39 mbsf (Site 1008). These horizons are characterized by nannofossil oozes that overlie cemented hardgrounds (see "Lithostratigraphy" section, this chapter) resulting in a spike-shaped velocity profile. The level of this SSB was dated in both holes at 0.4 Ma, which indicates an average duration of 100,000 years for the upper four seismic sequences, *s*–*v*.

Underlying Sequence *w* has a lower boundary at 126 and 53.2 mbsf at Sites 1009 and 1008, respectively. Its basal SSB W has an estimated age of 0.7 and 0.62 Ma, respectively. It might correlate at Site 1009 to a high-velocity layer 13 m higher in the cores, while it correlates with a smaller velocity peak at Site 1008.

The remaining lower sections of both holes show only two prominent velocity deviations from the background level, and both of them coincide with SSBs X and Y. SSB X (174 mbsf at 1009 and 77.4 mbsf at 1008) corresponds to a hardground at Site 1009 (178 mbsf) and with a thin, laminated, fine-grained unit overlying a thick, coarse layer at Site 1008 (78 mbsf). The assigned ages are 1.2 and 0.91 Ma, respectively, for Sites 1009 and 1008, which indicates some inconsistency in either the seismic or the biostratigraphic data. SSB Y occurs at a depth of 208 mbsf (Site 1009) and 126 mbsf (Site 1008), and it is likely that this reflection event is a result of high-velocity signatures observed at 220 and 122 mbsf, respectively. Site 1009 allows for a tentative age assignment of 1.3–1.4 Ma for SSB Y.

In summary, core to seismic correlation at Sites 1008/1009 documents how small-scale (5–30 m thickness) alternations of layers with contrasting physical properties can be imaged as individual seismic sequences on a high-resolution seismic data set. These alternations are interpreted to be caused by changes in sea level (see "Lithostratigraphy" section, this chapter) and document that the record of sea-level changes has an expression in the seismic sections. The recovered sediments indicate a higher number of cycles than seismic sequence boundaries, indicating that only a limited number of sea-level fluctuations are recorded in the seismic data. However, the good match between the number of major velocity spikes and the number of seismic sequences indicates that a certain hierarchy exists within the litholog-

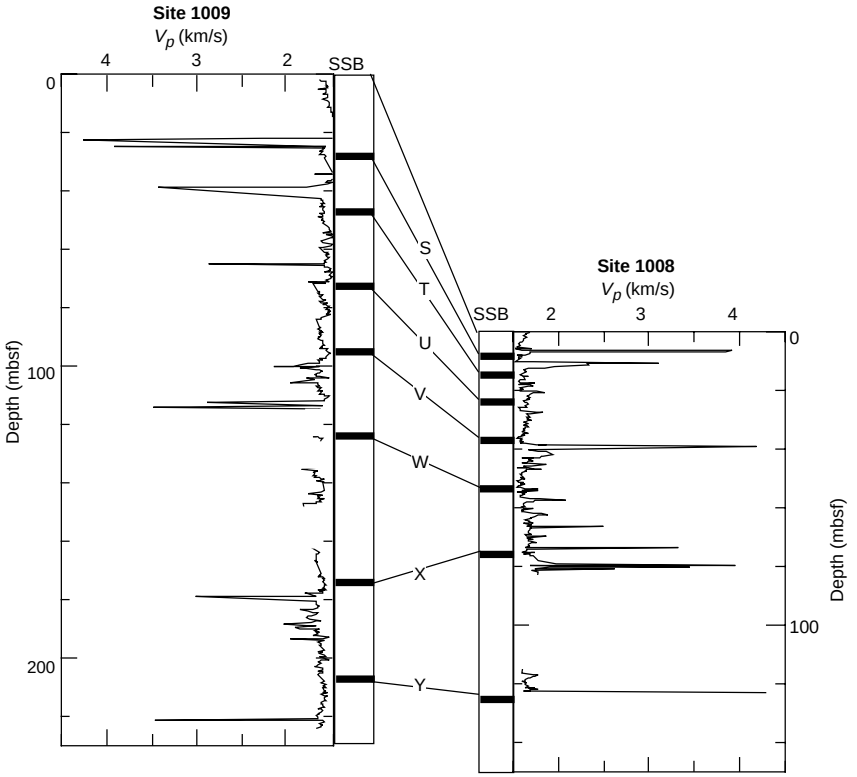

Figure 37. Correlation of seismic sequence boundaries (SSB) and DSV velocities (measured on split cores). Most of the SSBs coincide with distinct high-velocity spikes, which are caused by dark-colored, coarse, and cemented layers.

ic alternations, and that the major cycles are preferentially imaged in the seismic data.

SUMMARY AND CONCLUSIONS

Sites 1008 and 1009 penetrated thick Pleistocene sections of carbonate sediments, which consisted of unlithified to partially lithified peloidal and bioclastic mudstone, wackestone, and packstone with grainstone, floatstone intercalations, and nannofossil ooze. At Site 1008, the age at the base of the hole (134.5 mbsf) is younger than 1.44 Ma, with sedimentation rates varying between 4.5 and 16 cm/k.y. At Site 1009, a similar age was attained at a depth of 226.1 mbsf with rates between 5 and 55 cm/k.y. Pore-water geochemistry profiles showed a thick zone in which there were no changes in the concentrations of conservative and nonconservative elements. Below this zone, sulfate reduction and other diagenetic reactions were prevalent. Adara and WSTP temperature measurements revealed an irregular heat flux in the upper 40 mbsf and a much lower heat flux (20 mW vs. 40 mW) in the lower portion of the profile compared to Sites 1003–1007.

Sediment Age, Composition, and Sequence Stratigraphy

Sites 1008 and 1009 recovered expanded sections of Holocene and Pleistocene sediments. The nannofossil biostratigraphy indicates the presence of Zones NN19–NN21. The planktonic record is restricted to N22. Substantial reworking was found in the lower part of the cores. Two lithostratigraphic units were identified at both sites. Unit I, Holocene to latest Pleistocene in age, is composed of two subunits. Subunit IA consists of a coarsening-upward pale yellow to white unlithified peloidal wackestone grading into wackestone and mudstone, with minor to moderate bioturbation. Calcareous nannofossils are rare or absent in this subunit. The base of this subunit is marked in both sites by a bored and encrusted hardground. Subunit IB consists of multiple coarsening-upward units separated by layers of lithoclastic floatstones. These units are composed of unlithified peloidal mudstones at the base and peloidal packstones at the top. These correspond to cycles in physical properties. Characteristically, they have relatively low velocities, densities, and gamma ray at their base that increase toward the top. The floatstones contain large, gray lithoclasts composed of pteropod and planktonic foraminifer wackestone to packstone. The clasts are cemented and bored and are interpreted as being the remnant of a marine hardground. Subunit IC was not recognized at Site 1008. It contains four coarsening-upward intervals and is separated from Subunit IB by a fragmented hard layer consisting of pteropod biopackstone. Subunit IA at Site 1008 has a sedimentation rate of 4.5 cm/k.y. Subunit IB has a rate of 16 cm/k.y. At Site 1009, the sedimentation rates are 18 cm/k.y. throughout Subunit IA, up to 35 cm/k.y. in Subunit IB, and 7 cm/k.y. in Subunit IC. Unit II consists of unlithified lithoclastic and bioclastic floatstone. At Site 1009, two hardgrounds are recognized in this sequence. At Site 1008, the sedimentation rate in Unit II is 8 cm/k.y. At Site 1009, sedimentation rates are between 22 and 55 cm/k.y. throughout Unit II.

At both sites, a number of alternations in sediment composition, color, and mineralogy can be recognized, which probably correspond to sea-level changes. Lowstands are characterized by higher concentrations of LMC and darker colors, whereas highstands contain abundant aragonite and HMC. These alternations can be traced between the two sites. Dolomite becomes a minor component of the sediment below 60 mbsf at Site 1008 and 120 mbsf at Site 1009, and percent carbonate was generally higher than 95% throughout.

The youngest seismic sequence, *s*, appears at Site 1009 at 29 mbsf and at Site 1008 at 9.6 mbsf. The age of the SSB (0.15–0.12 Ma) probably corresponds to the last sea-level lowstand at the Pleistocene/Holocene boundary. SSB T corresponds to 48 mbsf at Site 1009 and 14.5 at Site 1008 and has an age of 0.20–0.25 Ma. These two boundaries as well as SSB U appear in both holes slightly deeper than high-velocity layers, allowing for the possibility that too high a velocity was assumed in these sediments for the time-depth conversion. Sequence *w* has its lower boundary at 126 and 53.2 at Sites 1009 and 1008, respectively. The associated age of SSB W is 0.7/0.62 Ma,

which might correlate to a high velocity layer 13 m higher in the core. The remainder of the holes show two prominent velocity deviations coinciding with SSBs X and Y.

Fluid Geochemistry

Based on the pore-water geochemistry, two distinct geochemical zones have been identified within sediments from Sites 1008 and 1009. An upper zone extends from the seafloor to a depth of 40 mbsf and is characterized by an absence of significant changes in the interstitial pore-water geochemistry. This flushed zone is similar to those observed at Sites 1006 and 1007, because there was slight evidence of carbonate recrystallization reactions in the form of a small, but nevertheless significant, increase in the Sr^{2+} concentration. The upper flushed zone merges into a region with elevated chlorinity, up to 730 mM at Site 1009 and 670 mM at Site 1008. This zone shows a small reduction in sulfate and large increases (up to 1600 µM) in Sr^{2+}. Calcium and magnesium are reduced relative to their seawater values in this interval, which suggests precipitation of carbonate minerals. Concentrations of methane and hydrogen sulfide reached 100 and 10,000 ppm, respectively, within the zone with low sulfate.

Heat flow at both sites is significantly lower than at Sites 1003–1007. At Sites 1008 and 1009, the geothermal gradients are approximately 27°C/km and 17°C/km, respectively. This compares to approximately 35°C/km for the northern sites. The low heat flow could suggest a regional cooling as a result of the inflow of bottom seawater, perhaps deeper in the sedimentary section.

Based on the chemical profiles from Sites 1008 and 1009, there appears to be a flushed zone similar to that encountered at the northern sites. The thickness of the flushed zone is comparable to that seen at Sites 1003–1005, although there appears to be either a slight reduction in the magnitude of the advection, or a higher rate of recrystallization in the southern sites. This is evident in the slight increase in the Sr^{2+} concentration in the flushed zone. The heat flow at Sites 1008 and 1009, however, is much lower than in the northern sites, a finding consistent with greater circulation of seawater through the margin. Therefore, there is an inconsistency between the heat flow and the chemical data, which suggests a greater degree of cooling at Sites 1008 and 1009 and a higher fluid flow. It is possible that what are being seen at the sites studied during Leg 166 are two different mechanisms of seawater advection, one common to both sites associated with the upper mixed zone and the other a more deep-seated flow only present at the southern sites, which depresses the regional heat flow.

REFERENCES

Baker, P.A., Gieskes, J.M., and Elderfield, H., 1982. Diagenesis of carbonates in deep-sea sediments: evidence from Sr^{2+}/Ca^{2+} ratios and interstitial dissolved Sr^{2+} data. *J. Sediment. Petrol.*, 52:71–82.

Claypool, G.E., and Kvenvolden, K.A., 1983. Methane and other hydrocarbon gases in marine sediment. *Annu. Rev. Earth Planet. Sci.*, 11:299–327.

Gaudett, H.E., And Lyons, W.B., 1980. Phosphate geochemistry in nearshore carbonate sediments: a suggestion of apatite formation. *In* Bentor, Y.K. (Ed.), *Marine Phosphorites: Geochemistry, Occurrence, Genesis.* Spec. Publ.—Soc. Econ. Paleontol. Mineral., 29:215–225.

Grammer, G.M., and Ginsburg, R.N., 1992. Highstand versus lowstand deposition on carbonate platform margins: insight from Quaternary foreslopes in the Bahamas. *Mar. Geol.*, 103:125–136.

Kitano, Y., Okumura, M., and Idogak, M., 1978. Uptake of phosphate ions by calcium carbonate. *Geochem. J.*, 12:29–37.

Mullins, H.T., 1983. Modern carbonate slopes and basins of the Bahamas. *In* Cook, H.E., Hine, A.C., and Mullins, H.T. (Eds.), *Platform Margin and Deep Water Carbonates.* Soc. Econ. Paleontol. Mineral. Short Course, 12:4-1–4-138.

Schlager, W., and James, N.P., 1978. Low-magnesian calcite limestones forming at the deep-sea floor, Tongue of the Ocean, Bahamas. *Sedimentology*, 25:675–702.

van Morkhoven, F.P.C.M., Berggren, W.A., and Edwards, A.S., 1986. Cenozoic cosmopolitan deep-water benthic foraminifera. *Bull. Cent. Rech. Explor.-Prod. Elf-Aquitaine*, Mem. 11.

Wilber, R.J., Milliman, J.D., and Halley, R.B., 1990. Accumulation of bank-top sediment on the western slope of Great Bahama Bank: rapid progradation of a carbonate megabank. *Geology*, 18:970–974.

Ms 166IR-111

Note: Core description forms ("barrel sheets") and core photographs can be found in Section 3, beginning on page 377. Forms containing smear slides can be found in Section 4, beginning on page 831. Thin-section descriptions can be found in Section 5, beginning on page 849. See the Table of Contents for material contained on CD-ROM.